ELSEVIER

Journal of Non-Crystalline Solids 197 (1996) 83–110

JOURNAL OF NON-CRYSTALLINE SOLIDS

Analysis of dispersed, conducting-system frequency-response data

J. Ross Macdonald *

Department of Physics and Astronomy, University of North Carolina Chapel Hill, NC 27599-3255, USA

Received 13 June 1995; revised 16 October 1995

Abstract

Widely used equations for the analysis of dispersive relaxation data for conducting materials, developed by Moynihan and associates more than two decades ago, are shown to be require correction. Corrected equations which can differ appreciably in their consequences from those of Moynihan et al. are derived and used to justify the empirical Barton, Nakajima, Namikawa (BNN) formula satisfied by much frequency-response data for disordered materials. The conductive-system frequency-response analysis described in the paper and the corrected Moynihan approach both allow arbitrary fitting models to be used. It is shown that, for one class of models, the two fitting approaches are identical and yield maximum information while, for other models, the fit information is intrinsically more limited and inaccurate. Improved methods for inverting transient-response data to yield the associated distribution of relaxation times and frequency response are compared with the approach Moynihan et al. used for the fractional-exponential fitting model (KWW), and a misconception in their work is corrected. Correct and incorrect ways to invert frequency-response data that include the effects of a high-frequency-limiting dielectric constant are illustrated for KWW response. The conventional KWW model yields physically unrealizable time and frequency responses, but a modification which restores realizability is developed. Analysis approaches are described which allow one to identify the type of dispersed behavior present in the data: either conductive- or dielectric-system response. Weighted, complex-non-linear-least-squares analyses of frequency-response data for $Li_2O–Al_2O_3–2SiO_2$ glass at 24°C using an approximate KWW fitting model are compared with earlier fitting results of the same data obtained by Moynihan and others using the Moynihan et al. equations and fitting approach. Excellent fits were obtained over the entire measured frequency range when the fitting model included elements accounting for electrode polarization effects in the data. These effects are shown to make non-negligible contributions at both extremes of the frequency-response range. Such contributions, and the past use of the Moynihan approach, probably explain most previously unexplained excess losses found present in the high frequency region, ones which Moynihan and associates characterized as endemic to the vitreous state.

1. Introduction

This work is concerned with methods of analysis of small-signal frequency-response data that involve dispersive conductivity-relaxation response. Such response is associated with the presence of mobile charges in a material and leads to a finite, non-zero dc conductivity. Widely used methods for analyzing dispersion in conductive systems, published more than 20 years ago by C.T. Moynihan and associates [1–5] (collectively referred to hereafter as CTM), are discussed and corrected. Alternative methods are

* Corresponding author. Tel: +1-919 967 5005; fax: +1-919 962 0480; e-mail: macd@gibbs.oit.unc.edu.

SSDI 0022-3093(95)00618-4

developed here; their usefulness for both synthetic and measured data is demonstrated; and their predictions are compared to the CTM ones. What Moynihan and his associates termed conductivity relaxation is here denoted as conductive-system relaxation. Since single-relaxation-time response is rarely seen in solids and liquids, the present work is concerned primarily with dispersed response. Discussion of the CTM approach, its corrected version, and their relationship to a general conductive-system approach are presented in Section 6 and in Appendix A. A list of acronyms used herein can be found in Appendix B.

Because the CTM work involves a distribution of conductivity relaxation times, and thus applies to conductive systems with dispersive behavior, it is important to distinguish between such systems and those with purely dielectric response, dispersed or otherwise [6–10]. To do so, the subscript 'C' will be used, when appropriate, to identify model response and response parameters arising from charge motion, and the subscript 'D' will be taken to designate those associated with dielectric response arising, for example, from induced and permanent dipoles present in the measured material and possibly even from non-percolating charges.

We shall be concerned with all four of the response levels routinely employed in impedance (more generally: immittance) spectroscopy (IS) [6,11]: the complex dielectric constant $\epsilon(\omega) = \epsilon'(\omega) - i\epsilon''(\omega)$; its inverse, the (electric complex) modulus, $M(\omega) = M'(\omega) + iM''(\omega)$; the impedance, $Z(\omega) = Z'(\omega) + iZ''(\omega)$ equal to $M(\omega)/(i\omega C_V)$; and its inverse, the admittance, $Y(\omega) = Y'(\omega) + iY''(\omega)$. Here ω is the angular frequency, and C_V is the capacitance of the empty measuring cell. For identical plane-parallel electrodes of area A and separation d, $C_V = \epsilon_V A/d$ where ϵ_V is the permittivity of vacuum. The subscript 'V' is used here rather than the more common 'o' or '0' to avoid confusion with quantities defined at $\omega = 0$. Further, the superscript asterisk, sometimes used to distinguish complex quantities such as ϵ or M from real-part quantities, is omitted as unnecessary here and also because it can be confused with the usual designation of the complex conjugate of a given complex quantity. The distinction between an immittance level and dispersive model response at a given level is an important one. One can express the response of a given model at any of the four levels, but such expression at one of these levels is often more instructive and usually more appropriate physically for a specific model than such representation at one of the other levels. Not only does immittance spectroscopy include electrochemical impedance spectroscopy and dielectric relaxation spectroscopy, but it also includes the small-signal ac response of semiconductors and biological materials as well [11].

Instead of using the impedance and admittance, it is often appropriate to use the complex resistivity, $\rho(\omega) = (C_V/\epsilon_V)Z(\omega) = \rho'(\omega) + i\rho''(\omega)$, here written with a positive sign for the imaginary part in order to agree with the conventional definition of the sign of $\mathrm{Im}[Z(\omega)]$. By contrast, the complex conductivity $\rho(\omega)^{-1}$ will be written as $\sigma(\omega) = (\epsilon_V/C_V)Y(\omega) = \sigma'(\omega) + i\sigma''(\omega)$. Then, for example, $M(\omega) = (i\omega\epsilon_V)\rho(\omega)$. No 'C' subscripts are needed for such quantities as ρ and σ since they are usually treated herein *as* intrinsically conductive-system quantities, but to allow possible distinction between the quantity $\rho'_{C\infty} \equiv \rho_{C\infty}$, introduced below, and $(\sigma_\infty)^{-1}$, the 'C' subscript will be used as shown. In accordance with common usage, I shall hereafter omit the single-prime superscripts from the dc resistivity, $\rho'_0 = \rho_0$, from its inverse, the dc conductivity $\sigma'(0) \equiv \sigma_0$, and from all frequency-independent parts of the resistivity and dielectric constant quantities. A caret will be used when it is desirable to distinguish between a model quantity and corresponding data. Thus $\epsilon(\omega)$ will represent model response and $\hat{\epsilon}(\omega)$ experimental data, both at the complex dielectric constant level.

In the past, dispersed response of a dielectric or conductive system has often been analyzed by writing $\sigma(\omega)$ in terms of a continuous distribution of weighted Debye-like processes [12–16]. Each such process may be considered to involve the response of a differential resistance in series with a differential capacitance, with all such processes in *parallel.* Since such a dielectric-system approach leads to $\sigma_0 = 0$, a separate treatment is required to obtain a non-zero expression for σ_0. By contrast, it is natural to express the response of a conductive system at the impedance (or complex resistivity) level in terms of a *series* combination of basic elements, each made up of the parallel combination of a differential resistance and a differential capacitance. Then, $Z'(0) \equiv R_0$, and ρ_0 and σ_0 are intrinsic parts of a unified calculation and are thus non-zero. When the parallel elements are not taken to be differential, one obtains a discrete, rather than continuous, distribution of relaxation times (the Voigt response circuit [11]). Analysis using a continuous or discrete distribution of relaxation times (DRT) model at the *Z*-level was suggested as early as 1956 for a conductive system by analogy to the corresponding dielectric DRT expression [6,17, p. 406]. The subsequent CTM *M*-level approach is closely related to such an analysis method. The above two disparate descriptions of relaxation response are often described as parallel and series approaches and are discussed in detail elsewhere [6,8,18]. Further, it has been shown [8], p. R60 and Fig. 6, that parallel or series structure can be alternatively represented exactly by sequential, i.e., hierarchical response structure. Finally, a unified approach to both types of descriptions has been proposed [6].

It is a truism, but, nevertheless, an important one, that the principal aim of experimental measurement is to gain knowledge and insight into the processes leading to the observed response. To do so usually requires the analysis of a parameterized model, one thought to incorporate at least the most important physicochemical processes occurring in the material system, including the electrodes. There has been considerable discussion concerning the virtue of analyzing conductive-system response at the modulus level (probably first introduced in the dielectric context by Schrama [19] in 1957, long before its use by CTM) or at one or another of the other three levels [20–23]. While it is always desirable to plot experimental data at all four of the IS levels, since the shapes of the resulting complex-plane curves and the semilog or log–log curves of the real and imaginary parts vs. frequency are often somewhat diagnostic of the dominant processes present [11], the choice of which level to use in analyzing the data is, in my opinion, largely a non-problem unless one wishes to identify whether the data arise from conductive-system or from dielectric-system response (see Section 8).

The reason why the choice of analysis at the impedance or modulus level is unimportant is as follows: all IS data should extend over as wide a frequency range as practical, and their real and imaginary (or modulus and phase) responses should be analyzed simultaneously with weighted, complex non-linear least square (CNLS) fitting of an appropriate model, yielding estimates of all parameters and of their standard deviations. The analyses of both simulated and experimental data in the present work use the very general and readily available CNLS program LEVM [24–27]. With proportional weighting (PWT), appropriate for constant-percentage random errors but independent of their presence, such fitting of ideal or non-ideal data with a given model shows that one obtains *exactly* the same fit, and *exactly* the same parameter estimates, whether the fit is carried out at the impedance level or the data and model are transformed to the modulus level before fitting.

Similar agreement is obtained for fitting at the dielectric-constant level and at the admittance level, where again the data differ only by a frequency-dependent weighting factor. Such exact agreement only occurs when both real and imaginary parts are fitted simultaneously with CNLS. For an exact match between noiseless data and a fitting model, fits at all four levels yield identical results, but for ordinary experimental data, where the errors in the data are moderate, the results for impedance-level and for admittance-level fitting are usually quite close. Fitting using CNLS allows one to avoid the cumbersome and inaccurate graphical and subtraction approaches to IS data analysis which are still frequently used [28–32]. It also provides a measure of the degree of fit of the model to the data based on the standard deviation of the residuals, S_F, and estimates of the uncertainties of the individual parameter estimates as well. Some examples of CNLS fitting of IS data appear in Refs. [7,9,10,26,27,33–38].

In accordance with the above definitions, $Z(\omega)$ will be used to denote the full impedance of a given response model, while $Z_C(\omega)$ will include only that part of it associated with conductive-system response. Finally, such quantities as $\epsilon_D(0) = \epsilon'_D(0) \equiv \epsilon_{D0}$ and $\epsilon_D(\infty) = \epsilon'_D(\infty) \equiv \epsilon_{D\infty}$ designate response at sufficiently low or high frequencies that extension of the frequency range in either direction leads to no change in model behavior in the extended region. Although it is quite possible that a given conducting material might show both conductive-type and dielectric-type dispersion within the frequency range available experimentally [9,38,39], in the present work I shall only be concerned with conductive-system dispersion, hereafter denoted by CSD, rather than dielectric-system dispersion (DSD). But all real materials, whether conductive or not, exhibit dielectric response, at least through the quantity $\epsilon_{D\infty}$. Here it will be assumed that any relaxation associated with such behavior occurs well beyond the highest measured frequency. Then, $\epsilon_{D0} = \epsilon_{D\infty}$, a quantity which must not be neglected [39].

It has not always been fully realized that CSD alone can often lead to important contributions to the overall dielectric constant. Thus, one needs to introduce the quantities ϵ_{C0} and $\epsilon_{C\infty}$, where $\epsilon_{C0} > \epsilon_{C\infty}$ for dispersive response. The full low-frequency limiting dielectric constant of such a system can then be written as $\epsilon_0 = \epsilon_{C0} + \epsilon_{D\infty}$. Similarly, $\epsilon_\infty = \epsilon_{C\infty} + \epsilon_{D\infty}$. Note that if one defines $\Delta\epsilon$ as $\epsilon_0 - \epsilon_{D\infty}$, it here equals ϵ_{C0}, a purely conductive-system quantity under the present assumptions, even though it formally seems to specify the strength of a dispersion process at the dielectric level. In many treatments of conductivity dispersion (conductive-system response), ϵ_0 has just been defined as the low-frequency limiting value of the dielectric constant without discussion or explicit recognition of its provenance and possible components.

2. The CTM equations for a dispersed conductive system

Sufficient background has now been provided that the CTM equations [1–5], mentioned above, may be written in the present notation as

$$\sigma_0 \langle \tau \rangle_D = \epsilon_V \epsilon_{D\infty}, \tag{1}$$

$$\sigma_\infty \left[\langle \tau^{-1} \rangle_D \right]^{-1} = \epsilon_V \epsilon_{D\infty}, \tag{2}$$

and

$$\epsilon_{C0} \left[\left\{ \langle \tau^2 \rangle_D / \langle \tau \rangle_D^2 \right\} - 1 \right]^{-1} = \epsilon_{D\infty}, \tag{3}$$

where

$$\langle \tau^m \rangle_D \equiv \int_0^\infty \tau^m g_D(\tau)\, d\tau. \tag{4}$$

In forming the above relations, the equation $\epsilon_0 = \epsilon_{C0} + \epsilon_{D\infty}$ has been used. The subscript 'D' here indicates that the DRT, $g_D(\tau)$, is that defined for dielectric (parallel) response. It is usually normalized.

Eqs. (1)–(3) have been written so that purely conductive quantities appear on the left and purely dielectric ones on the right. These equations thus directly connect quantities associated with entirely different physical processes with each other, physically implausible except in the case of only a single relaxation time where one deals only with definitions. For example, such a single-relaxation-time definition is [1] $\tau_\sigma \equiv \epsilon_V \epsilon_{D\infty} / \sigma_0$. Of the above expressions, Eq. (1) has been the one most used for data analysis since its genesis, particularly to estimate σ_0 from an estimate of $\epsilon_{D\infty}$ when an estimate of $\langle \tau \rangle_D$ is available. Although the above results are not usually expressed in terms of purely conductive quantities, they can be combined to yield

$$\sigma_\infty = \langle \tau \rangle_D \langle \tau^{-1} \rangle_D \sigma_0, \tag{5}$$

and

$$\epsilon_{C0} = (\sigma_0/\epsilon_V) \langle \tau \rangle_D \left[\left\{ \langle \tau^2 \rangle_D / \langle \tau \rangle_D^2 \right\} - 1 \right]. \tag{6}$$

Corrections to some of these equations are derived in Appendix A.

3. A new analysis of the limiting responses of a dispersed conducting system

To derive equations to compare with those of CTM and to see how to correct the latter when possible, it is necessary to obtain the low- and high-frequency limiting responses at the complex conductivity and dielectric levels arising from CSD. In order to maintain close contact with an actual equivalent circuit, I shall initially deal with quantities such as resistances and capacitances and then transform the results to resistivities, conductivities, and dielectric constants. Conductive-system response can be most generally expressed in terms of a non-dispersed, possibly non-zero, high-frequency-limiting resistance, R_∞ [10,38]; the strength of the dispersion process, $\Delta R \equiv R_0 - R_\infty$; and a normalized relaxation/dispersion Z-level response function, $I(\Omega) = I'(\Omega) + iI''(\Omega)$ [6]. Here R_0 is the limiting low-frequency resistance of the system; $\Omega \equiv \omega\tau_o$; $I(0) = 1$; and $I(\infty) = 0$. No 'C' subscript is usually needed for the function $I(\Omega)$, since only conductive-system relaxation/dispersion is assumed to be present. The normalized frequency Ω should not be confused with the symbol for ohms. The relaxation time τ_o is specified as part of the frequency- or transient-response function. It follows that one can define the conductive-system model response at the impedance level as

$$Z_C(\Omega) = R_\infty + \Delta R I(\Omega). \tag{7}$$

But any real material involves dielectric response as well. Thus, for the present situation one must include a capacitance $C_{D\infty} \equiv C_V \epsilon_{D\infty}$ in parallel with Z_C, thus defining the full model response $Z(\Omega)$.

Let us now write an expression for this full response at the complex conductivity level, one including the effect of $\epsilon_{D\infty}$ as well as $Z_C(\Omega)$ and expressed in terms of Ω rather than ω. To do so, resistances are transformed to resistivities and capacitances to dielectric constants. Then one obtains
We next need to develop expressions for the $\Omega \to 0$ and $\Omega \to \infty$ limits of the real and imaginary parts of $\sigma(\Omega)$ and $\epsilon(\Omega)$, and so of those of $I(\Omega)$. It will be assumed hereafter that the conductive-system response involves a continuous DRT. There are several ways in which such a DRT can be written, and it is important to specify which form is being used in a given situation. This matter is further discussed in Section 5. Here, it is necessary to distinguish between the CTM $g_D(\tau)$ distribution and the conventional one, $G(\tau)$, often defined for Z-level CSD response [17, pp. 401–402;27,40,41]. Further, let us define $x \equiv (\tau/\tau_o)$ in order to avoid the need to use such mathematical solecisms as $\log(\tau)$. It will then be convenient to deal with the distribution of x rather than τ. The corresponding DRT, $G_x(x)$, satisfies the relation $G(\tau)|d\tau| = G_x(x)|dx|$ by conservation of probability. It follows that $G_x(x) = \tau_o G(\tau)$. When only a single relaxation time is present, as in simple Debye relaxation, $G_x(x) = \delta(x-1)$.

First, let us express the normalized frequency-response function in terms of a DRT at the Z-level [6,17, p. 406], in general form as

$$I(\Omega) = \int_0^\infty \frac{G_x(x)\,dx}{[1 + i\Omega x]}, \tag{9}$$

since $\omega\tau = \Omega x$. Note that G_x is normalized when $I(0) = I'(0) = 1$, as it is here. Let us now write the analog of Eq. (4) as

$$\langle x^m \rangle \equiv \int_0^\infty x^m G_x(x)\,dx, \tag{10}$$

equal to unity for any m when there is only a single relaxation time. The averages defined by Eq. (10) are pure functions of the shape of the G_x distribution, independent of τ_o.

From Eqs. (9) and (10), we can now derive the general CSD relations

$$\lim_{\Omega \to 0} \left[-\Omega^{-1} I''(\Omega) \right] = \langle x \rangle, \tag{11}$$

$$\lim_{\Omega \to 0} \left[\Omega^{-2} \{1 - I'(\Omega)\} \right] = \langle x^2 \rangle, \tag{12}$$

$$\lim_{\Omega \to \infty} \left[-\Omega I''(\Omega) \right] = \langle x^{-1} \rangle, \tag{13}$$

and

$$\lim_{\Omega \to \infty} \left[\Omega^2 I'(\Omega) \right] = \langle x^{-2} \rangle. \tag{14}$$

For physically realizable response [39,42], such as that of a Gaussian distribution of activation energies [7,8], all the above averages are finite and non-zero. Specific expressions for them are calculated for a physically realizable form of the important KWW fractional-exponential response function [43–45] in Appendix C. Its fractional exponent will be denoted by β or β_D.

Eqs. (8)–(14) now lead to the result

$$\lim_{\Omega \to 0} \mathrm{Re}[\epsilon(\Omega)] \equiv \epsilon_0 = \epsilon_{D\infty} + \left(\tau_o \Delta\rho / \epsilon_V \rho_0^2\right)\langle x \rangle, \tag{15}$$

and so

$$\epsilon_C(0) \equiv \epsilon_{C0} = \left(\tau_o \Delta\rho / \epsilon_V \rho_0^2\right)\langle x \rangle, \tag{16}$$

an important result for a quantity likely to have only weak temperature dependence (see the discussion in the following section). Note that $\tau_o^m \langle x^m \rangle \equiv \langle \tau^m \rangle$ and that when $\rho_{C\infty} = 0$, we may replace $\Delta\rho/\rho_0^2$ by σ_0. Then

$$\sigma_0 \langle \tau \rangle = \epsilon_V \epsilon_{C0}, \tag{17}$$

different from even the corrected version of the CTM Eq. (1) (see Appendix A). Now we see that the entire equation involves only conductive-system quantities, as it should. Further, Eq. (16) predicts values of ϵ_{C0} which need not be negligible compared to $\epsilon_{D\infty}$. For example, if $\rho_{C\infty} = 0$, $\tau_o \simeq 8.854 \times 10^{-4}$ s, $\rho_0 = 10^8$ Ω cm, and $\langle x \rangle = 6$, then $\epsilon_{C0} = 600$.

The calculation of ϵ_∞ is not quite so straightforward, since we must distinguish between the $\rho_{C\infty} \neq 0$ and $\rho_{C\infty} = 0$ cases. When $\rho_{C\infty} > 0$ one finds just

$$\lim_{\Omega \to \infty} \mathrm{Re}[\epsilon(\Omega)] \equiv \epsilon_\infty = \epsilon_{D\infty}. \tag{18}$$

For $\rho_{C\infty}$ identically zero, one obtains

$$\epsilon_\infty = \epsilon_{D\infty} + (\tau_o \sigma_0/\epsilon_V)[\langle x^{-1} \rangle]^{-1}, \tag{19}$$

so that then

$$\epsilon_{C\infty} = (\sigma_0/\epsilon_V)[\langle \tau^{-1} \rangle]^{-1}. \tag{20}$$

Eqs. (16) and (20) then yield for $\epsilon_{C\infty} > 0$,

$$\epsilon_{C0} = \epsilon_{C\infty}[\langle \tau \rangle \langle \tau^{-1} \rangle], \tag{21}$$

different results than the CTM ones of Eqs. (2) and (3) (see Appendix A). Although $\epsilon_\infty = \epsilon_{D\infty}$ when $\rho_{C\infty} > 0$, there may nevertheless be an appreciable frequency region where $\epsilon'(\Omega) \simeq \epsilon_{D\infty} + \epsilon_{C\infty}$ before its final drop to $\epsilon_{D\infty}$.

The above results also allow us to obtain quite general limiting expressions for $\sigma'(\Omega)$. Eqs. (8)–(14) lead to

$$\lim_{\Omega \to 0} \mathrm{Re}[\sigma(\Omega)] \equiv \sigma_0 = 1/\rho_0, \tag{22}$$

and for $\rho_{C\infty} \neq 0$ to

$$\lim_{\Omega \to \infty} \mathrm{Re}[\sigma(\Omega)] \equiv \sigma_\infty = 1/\rho_{C\infty}, \tag{23}$$

and for $\rho_{C\infty} = 0$ to

$$\sigma_\infty = \sigma_{C\infty} \equiv \sigma_0 \frac{\langle x^{-2} \rangle}{[\langle x^{-1} \rangle]^2}. \tag{24}$$

Even when $\rho_{C\infty} \neq 0$ and $\sigma_{C\infty} \ll 1/\rho_{C\infty}$, there may be an appreciable range of frequencies at which $\sigma'(\Omega)$ is close to $\sigma_{C\infty}$ before it finally approaches $1/\rho_{C\infty}$. Although physical realizability requires that $\sigma_\infty < \infty$, the final limiting value can arise either from a non-zero $\rho_{C\infty}$ or from $\sigma_{C\infty}$ when $\rho_{C\infty} = 0$. Because of a formal duality between CSD and DSD response expressions [6], all the above CSD limiting expressions have DSD counterparts (involving the moments of the DSD distribution), but they are usually not of much interest and importance.

There are many time constants which can be formed using the quantities above. Two important ones are $\tau_{C0} \equiv \epsilon_V \epsilon_{C0} \rho_0$ and, for $\rho_{C\infty} = 0$, $\tau_{Cm} \equiv \epsilon_V \epsilon_{C\infty}/\sigma_{C\infty}$. Then,

$$\tau_{C0}/\tau_o = \langle \tau/\tau_o \rangle = \langle x \rangle, \tag{25}$$

and

$$\tau_{Cm}/\tau_o = \langle x^{-1} \rangle / \langle x^{-2} \rangle. \tag{26}$$

Thus, $\tau_{C0} \geq \tau_o$ and $\tau_{Cm} \leq \tau_{C0}$.

4. The BNN relation and two identification problems

The BNN relation [10,21,46–48] is an empirical equation which is satisfied for many glasses and is somewhat similar in form to Eq. (17) above. If one defines $\tau_{CDp} \equiv \omega_{CDp}^{-1}$, where ω_{CDp} is the angular frequency of the dielectric loss peak (obtained by transforming $\hat{\rho}(\omega)$ or $\hat{\sigma}(\omega)$ data to the dielectric level and forming $\hat{\epsilon}_s''(\omega)$ by the relation $\hat{\epsilon}_s''(\omega) \equiv \hat{\epsilon}''(\omega) - \sigma_0/\omega\epsilon_V$), then the BNN expression is

$$\sigma_0 \tau_{CDp} = p \epsilon_V \Delta\epsilon, \tag{27}$$

where p is a nearly temperature-independent constant often found to be close to one in value. Here $\Delta\epsilon$ is the full experimental or model value, $\epsilon_0 - \epsilon_\infty$, which, from the above analysis, can involve ϵ_{C0}, $\epsilon_{C\infty}$ and $\epsilon_{D\infty}$, although $\epsilon_{C\infty}$ may be negligible compared to $\epsilon_{D\infty}$. Although for CSD τ_{CDp} is not a dielectric-system quantity but rather a conductive-system one, its calculation at the dielectric level is here indicated by the extra subscript 'D'.

The near temperature independence of p indicates that for a thermally activated situation the activation energies of σ_0 and τ_{CDp} must be nearly equal. In charge hopping situations, it has been shown that σ_0

and the hopping rate have essentially the same activation energy when the carrier concentration is not thermally activated [49,50]. Since $\tau_{\mathrm{CD}p}$ should be closely related to the inverse of the hopping rate, it is not surprising that the above activation energies are comparable in such situations. Finally, experimentally determined values of $\Delta\epsilon$ are often found to be proportional to T^{-1}, where T is the absolute temperature [48].

Comparison of the above expression with Eq. (17) shows that when the latter applies it provides a theoretical rationale for BNN experimental behavior and leads when $\epsilon_{\mathrm{C}\infty}$ is neglected, to

$$p = \tau_{\mathrm{CD}p}/\langle\tau\rangle = (\tau_{\mathrm{CD}p}/\tau_{\mathrm{o}})/\langle x\rangle; \qquad (28)$$

thus p should depend on the shape of the dispersion, which will often be a relatively weak function of temperature, and on the difference between $\tau_{\mathrm{CD}p}$ and τ_{o}. Although this difference also depends on the specific response model and could show some small temperature dependence, the p of Eq. (28) should indeed be nearly temperature independent for most conductive-system, thermally activated materials. For conductive-system KWW response with $\beta = 0.5$, $\tau_{\mathrm{CD}p}/\tau_{\mathrm{o}} \simeq 3.1$ and $\langle x\rangle = 6$ yielding $p \simeq 0.5$. Note that for the present situation the conductive-system ratio $\tau_{\mathrm{C}p}/\tau_{\mathrm{o}} \simeq 1.3$, where $\omega_{\mathrm{C}p}\tau_{\mathrm{C}p} = 1$ and $\omega_{\mathrm{C}p}$ is the value at the peak of the $-Z''_{\mathrm{C}}(\omega)$ or $-\rho''_{\mathrm{C}}(\omega)$ curve. Finally, unless $\Delta\epsilon$ and $\epsilon_{\mathrm{D}\infty}$ should happen to be comparable in size, one would not expect the CTM Eq. (1) expression to yield a very plausible value of p.

There are two important identification problems. The first is to decide whether to represent dispersed data by a conductive-system model where ρ_0, or at least $\Delta\rho$, is an intrinsic part of the dispersion model defined at the complex resistivity or modulus level, or to represent the data by a dispersion model which does not involve σ_0 intrinsically. The latter choice, the conventional dielectric dispersion one, assumes ''that one is dealing with a dielectric effect with a dc conductance in parallel'' [28]. This assumption is certainly appropriate for a leaky dielectric material with a distribution of dielectric relaxation times. It is, then, often represented formally by means of a DRT expressed at the dielectric level (or essentially equivalently, at the complex conductivity level). Dielectric dispersion involving induced or permanent dipoles may not be appreciably thermally activated, or, if $\tau_{\mathrm{CD}p}$ is activated [51], such activation should be unrelated to that of σ_0. Thus, data analysis at several temperatures should allow one to distinguish between the two possibilities. Since the dc resistivity and relaxation times of a conductive system are nearly always activated, when they are found to have nearly the same activation energy it is obviously appropriate to carry out the analysis at the complex resistivity level, contrary to most past practice. See Section 8 for further discussion of identification methods for the present problem.

The above conclusions suggest that it is unnecessary to test conductive-system results against the BNN equation, instead Eq. (17) is sufficient. One only needs to calculate $\hat{\epsilon}''_{\mathrm{s}}$ when one wants to examine its dependence on frequency, usually to see to whether it is nearly frequency-independent over some range and thus is likely to be associated with dielectric-system dispersion, especially at low temperatures [38]. When such dispersion is negligible, the results of a CNLS fit to a full conductive-system response model may be used to compare data and fit predictions and to calculate $\epsilon_{\mathrm{C}0}$. There are two ways the quantity $\langle x\rangle$ needed in the latter calculation may be estimated when the data fit the model adequately. First, it can often be calculated directly from the form of the main response function used in the fitting, such as the KWW model (see Appendices A and C). Alternatively, LEVM may be used to invert available time or frequency-response data (synthetic or experimental) to obtain a direct estimate of the DRT associated with the data [27]. As part of such a LEVM fit, all $\langle x^{\mathrm{m}}\rangle$ values defined in Section 3 are automatically calculated.

The second identification problem is that of distinguishing between the various components of ϵ_0 and ϵ_∞. Part of the problem arises because Maxwell's equations do not allow one to distinguish directly between convection and displacement currents in experimental ac measurements. Although the quantities involving a 'C' subscript involve convection and those with a 'D' subscript involve displacement processes, we can, nevertheless, distinguish them because of the different frequency responses of conductive and dielectric processes. Consider the fitting of frequency-response data arising from the presence of $\epsilon_{\mathrm{D}\infty}$ but no DSD, and from conductive-system response of the form of the Z_C of Eq. (7). Further, for concreteness, assume that $I(\omega)$ may be adequately represented by the KWW response model. Then CNLS fitting will yield estimates of $\epsilon_{D\infty}$, $\rho_{C\infty}$, $\Delta\rho$, τ_o, and β.

If fitting leads to a zero estimate for $\rho_{C\infty}$, then comparison of the experimental value of ϵ_∞ in a final high-frequency plateau region with that of $\epsilon_{D\infty}$ should show whether $\epsilon_{C\infty}$ is negligible or not. Alternatively, with a non-zero estimate of $\rho_{C\infty}$ and a sufficiently wide frequency range, one may be able to identify the decrease from $\epsilon_{C\infty}+\epsilon_{D\infty}$ to $\epsilon_{D\infty}$ if $\epsilon_{C\infty}$ is not negligible compared to $\epsilon_{D\infty}$. Next, the measured parameters allow one to calculate ϵ_{C0}. When no electrode effects are present, this value should agree well with $\epsilon_0-\epsilon_{D\infty}$. If it does not, and $\epsilon'(\omega)$ increases rapidly above this value as ω is decreased, then one should add electrode polarization components to the fitting model to account for such a rise [11,28,39]. Fitting once more with such components included should yield a much improved fit of the complete data set. Their effect can then be eliminated from the data (as described in Section 8), and the modified $\epsilon'(\omega)$ data then compared with the calculated value of ϵ_{C0} at the low-frequency end of the measurements. Finally, measurements of a conducting system material with two or more different values of doping (and so with different values of σ_0) can help one separate the $\epsilon_{C\infty}$ and $\epsilon_{D\infty}$ contributions to ϵ_∞, and perhaps also any dielectric constant and conductivity contributions associated with non-percolating charges hopping over a barrier between two states [9,10].

5. DRT and other response relations

The standard linear-system relations have been developed primarily for analyzing dielectric response, and even these relations are not always given in consistent form, e.g. [40]. Here, we need equivalent relations appropriate for a conductive system. Some such relations were summarized in a 1956 review of linear-system integral transform relations [17], and some appear in the CTM work and elsewhere [1–4,40,41,52]. In particular, we need relations connecting frequency response at the impedance level with a DRT and with the corresponding time-domain transient response. Such relations cannot all be directly transcribed from those that apply for dielectric-system response.

Let us first consider the transient-response function, $B(t)$, whose Laplace transform yields Z_C. $B(t)$ is the response to an impulse-function driving force. The corresponding function, $A(t)$, is the response of the system to a step function. These quantities are related by [17, p. 395]

$$B(t)=A(0)\delta(t)+\mathrm{d}A(t)/\mathrm{d}t. \tag{29}$$

For the present situation, it is appropriate to define $A(0)$ as R_∞ and set

$$A(t)=R_\infty+\Delta R\{1-f(t)\}, \tag{30}$$

with $f(0)=1$ and $f(\infty)=0$; then $A(\infty)=R_0$. It then follows from Eqs. (29) and (30) that

$$Z_C(p)=\int_{0-}^{\infty}B(t)\exp(-pt)\,\mathrm{d}t=R_\infty+\Delta R I(\omega), \tag{31}$$

where here

$$I(\omega)=\int_{0-}^{\infty}(-\mathrm{d}f(t)/\mathrm{d}t)\exp(-pt)\,\mathrm{d}t. \tag{32}$$

The Laplace variable p may be taken as $\mathrm{i}\omega$ here. The present normalized $f(t)$ is equivalent to the $\phi(t)$ relaxation function (actually a retardation function [53]) used in much previous dielectric- and conductive-system work. It describes the return to equilibrium of the system after a perturbation. For a single relaxation time, $\tau_o\equiv\Delta\rho\epsilon_v\epsilon_{D\infty}$, and one may take $f(t)=\exp(-t/\tau_o)$ and obtain $I(\omega)=1/(1+\mathrm{i}\omega\tau_o)$.

The remaining equations needed, written in terms of τ rather than x, are [12,41,52]

$$f(t)=\int_0^\infty G(\tau)\exp(-t/\tau)\,\mathrm{d}\tau, \tag{33}$$

and, from Eq. (9),

$$I(\omega)=\int_0^\infty\frac{G(\tau)\,\mathrm{d}\tau}{[1+\mathrm{i}\omega\tau]}. \tag{34}$$

Since most IS temporal or frequency-response data cover many decades of time or frequency, one usually uses equal or approximately equal intervals of the variable $y\equiv\ln(x)$, rather than such intervals of the x or τ variables, for actual DRT calculations.

Note that for a thermally activated system, y may be interpreted in terms of the activation energy. When Eqs. (33) and (34) are rewritten in terms of y, one obtains

$$f(t) = \int_{-\infty}^{\infty} \tau G(\tau) \exp(-t/\tau) \, d\{\ln(\tau/\tau_o)\}$$
$$= \int_{-\infty}^{\infty} F(y) \exp\{-(t/\tau_o) \exp(-y)\} \, dy, \tag{35}$$

and

$$I(\omega) = \int_{-\infty}^{\infty} \frac{\tau G(\tau) \, d\{\ln(\tau/\tau_o)\}}{[1 + i\omega\tau]}$$
$$= \int_{-\infty}^{\infty} \frac{F(y) \, dy}{[1 + i\omega\tau_o \exp(y)]}, \tag{36}$$

since $F(y) = \tau G(\tau)$ from conservation of probability, and $F(y)$ is essentially a distribution of activation energies for a distributed, thermally activated situation. It is particularly necessary to distinguish between the DRT forms $G(\tau)$ and $F(y) = H(x) \equiv \tau G(\tau)$. Comparison of Eqs. (33) and (34) with related equations in the CTM work [4] shows that their $g(\tau) \equiv g_D(\tau)$ and the present $G(\tau)$ may sometimes be taken equivalent when a continuous distribution is being considered (see Appendix A).

6. Identification and correction of the CTM analysis errors, and inversion of discrete data

The CTM modulus-level approach [1–5] has been and continues to be widely employed for conductive-system data analysis (see, for example Refs. [23,29,32,50,54–61]). This approach, which does not include consideration of a non-zero R_∞ and does not recognize the existence of such a CSD quantity as $\epsilon_{C\infty}$, begins with a correct expression for the $M(\omega)$ response associated with the capacitance, $C_{D\infty}$, and the resistance corresponding to the dc conductivity, σ_0. The CTM single relaxation time, termed τ_σ, and equal to $\epsilon_V \epsilon_{D\infty}/\sigma_0$, was properly identified as the Maxwell relaxation time for an RC circuit. CTM then directly generalized their $M(\omega)$ expression to involve a DRT at the complex modulus level, obtaining

$$M_{CTM}(\omega) = (\epsilon_{D\infty})^{-1} \int_0^{\infty} \frac{i\omega\tau g_D(\tau) \, d\tau}{[1 + i\omega\tau]}$$
$$= (\epsilon_{D\infty})^{-1} [1 - I_D(\omega)], \tag{37}$$

similar to a distributed high-pass response function proposed earlier [17, p. 407]. The rightmost expression in this equation appears in the CTM work [4] with the present $I_D(\omega)$ denoted there by $N^*(\omega)$. Because $g_D(\omega)$ is normalized to unity, Eq. (37) leads to $M'_{CTM}(\infty) = 1/\epsilon_{D\infty}$, an incorrect result for CSD, as demonstrated in Appendix A and discussed briefly earlier [26]. As shown in this Appendix, the CTM generalization error may be corrected by changing $\epsilon_{D\infty}$ in Eq. (37) to $\epsilon_{C\infty}$, a change leading to numerous important consequences.

To help illuminate the difference between the original CTM approach and an associated CSD approach, let us write the $Z_C(\Omega)$ expression following from Eqs. (7) and (34) at the M-level with $R_\infty = 0$ and $G(\tau)$ set equal to the DSD distribution expression $g_D(\tau)$. The result is

$$M_C(\omega) = (\epsilon_V \rho_0) \int_0^{\infty} \frac{i\omega g_D(\tau) \, dt}{[1 + i\omega\tau]}$$
$$= (i\omega\epsilon_V/\sigma_0) I(\omega), \tag{38}$$

where the CSD normalized response function $I(\omega)$ is not generally the same as $I_D(\omega)$. If, however, we assume that they are the same and set the rightmost side of Eq. (37) directly equal to the rightmost part of Eq. (38), we obtain, on solving for $I(\omega)$, the undispersed result $I(\omega) = 1/(1 + i\omega\tau_\sigma)$, the original single-time-constant response.

Note that Eq. (38) does not include the τ present in the numerator of the integrand of Eq. (37), and Eq. (38) does not involve ϵ_∞, since it represents only that part of the total response involving pure CSD. In fact, one can show with the help of Eqs. (10) and (20) that $M'_C(\infty) = 1/\epsilon_{C\infty}$, as one would expect. When CSD is present, even if $R_\infty = 0$, it is improper to include $C_{D\infty}$ as an integral part of the dispersive response, as in the original CTM approach. When the DRT is continuous rather than discrete, CSD response can be represented by a transmission line made up of an infinite number of individual differential R s and C s in parallel, all in series (similar to the Voigt response model for discrete elements). Taking $C_{D\infty}$ separate from these series Cs is quite different from melding it into them somehow when the DRT is continuous or even if there is more than one discrete RC pair present.

A CSD data-fitting approach employing Eq. (37) with $\epsilon_{D\infty}$ replaced by $\epsilon_{C\infty}$ will be designated by CTM hereafter (usually omitting the word 'corrected'), and one using Eq. (34) or Eq. (38), with an arbitrary DRT, by CSD. Note that when a fitting model is available in normalized form, i.e., $I_D(\omega)$ or $I(\omega)$, but integration using the (possibly unknown) associated DRT is inconvenient or impractical, one can use the model directly in the right-hand-sides of the corrected Eq. (37) or (38) for CNLS fitting. These possibilities are further compared in Appendix A.

Finally, it is worth remarking that if data sets at different temperatures are found to be well fitted by CTM and lead to values of an estimated fractional exponent, say β_D for the KWW $g_D(\tau)$ distribution, which, for example, decreases with increasing temperature, then the estimated β values obtained from Eq. (38) CSD fitting results of the same sets will be found to increase with increasing temperature. However, for DSD response, the high-frequency-limiting log–log slope of $\sigma'(\omega)$ vs. $\beta_{DM} \equiv 1-\beta_D$ for the KWW fitting model, and therefore the temperature dependence and magnitude of this quantity should be comparable to that of the CSD-fit β, even though the CTM approach is essentially a CSD, not DSD, one.

In a complete treatment of CSD response, $C_{D\infty}$ is in parallel with Z_C,and one must write for the full system when $R_\infty = 0$

$$M(\omega) = i\omega C_V Z_C/(1+i\omega C_{D\infty} Z_C) = M_C(\omega)/\left[1+\epsilon_{D\infty} M_C(\omega)\right]. \tag{39}$$

When $\omega \to \infty$, this expression leads to $M(\infty)^{-1} = \epsilon_\infty \equiv \epsilon_{C\infty} + \epsilon_{D\infty}$.

The actual CTM data analysis procedure [4] approximates possibly continuous $G(\tau)$ distributions by a sum of discrete ones but does not include an estimate of the errors in the estimated distributions which occur when $G(\tau)$ is continuous, as it is in the KWW case they considered. Such approximation is equivalent to replacing a continuous DRT, $G(\tau)$, by $\sum_{m=1}^{M} g_m \delta(\tau-\tau_m)$ and $F(y)$ by the equivalent result, $\sum_{m=1}^{M} d_m \delta(y-y_m)$, where the g_m and d_m coefficients specify the strength of each discrete relaxation process at each τ_m value, and M is the total number of such coefficients. When these discrete-distribution expressions are substituted in Eqs. (34) to (36), one obtains

$$f(t) = \sum_{m=1}^{M} g_m \exp(-t/\tau_m), \tag{40}$$

$$I(\omega) = \sum_{m=1}^{M} \frac{g_m}{[1+i\omega\tau_m]}, \tag{41}$$

$$f(t) = \sum_{m=1}^{M} d_m \exp\{-(t/\tau_o)\exp(-y_m)\}, \tag{42}$$

and

$$I(\omega) = \sum_{m=1}^{M} \frac{d_m}{[1+i\omega\tau_o \exp(y_m)]}, \tag{43}$$

where the choice of τ_o is arbitrary. These equations are exact for true discrete distributions.

In order to obtain estimates of the g_m coefficients from temporal data, CTM set the right side of Eq. (40) equal to the DSD KWW response function,

$$f(t) = \exp\left[-(t/\tau_o)^\beta\right], \tag{44}$$

with $0<\beta\le 1$. This KWW inversion approach was proposed earlier by Majumdar [62], who used Eq. (33) to estimate a continuous $G(\tau)$ for KWW stress relaxation in glass. Although Majumdar obtained a closed-form approximation for $G(\tau)$, the CTM analysis, which employed linear least-squares fitting, actually led to an approximation not of $G(\tau)$ but of the $F(y)$ or $H(x)$ distributions of Eq. (36). Although the CTM distribution coefficients were identified as the g_ms of Eqs. (40) and (41), CTM actually used logarithmic variables, thus making Eqs. (42) and (43) appropriate and yielding the d_m coefficients appearing in these equations. The truth of these statements is further demonstrated by the results of the next section. Finally, once an estimate of a DRT is available, it can be used in Eqs. (33) or (34) or (40)–(43) to generate the estimated approximate associated time or frequency response. This is the approach developed by CTM [4] to allow fitting of the KWW model for any value of β within its range to experimental IS data. As discussed below, different and often better alternatives to this specific task have existed for some time.

In passing, however, it is worth emphasizing that the transformation of measured temporal (frequency) response data to the frequency (time) domain, usually accomplished by means of a fast Fourier transform [63], may often be carried out in simpler and more accurate fashion by using the intermediary of DRT estimation (employing the continuous-distribution analogs of Eqs. (42) and (43), as incorporated in LEVM [27]; see the discussion in the next section). Fourier analysis of discrete data not only yields results different from such transformation of an equivalent continuous function [64], but it is cumbersome and difficult to apply when the data range extends over many decades. Alternatively, when inversion of the data in a given domain can be carried out to estimate the $\{d_m, \tau_m\}$ DRT set with a sufficiently large value of M, good estimates of the response in the other domain may be directly calculated.

7. Estimation of the KWW distribution functions and frequency response

7.1. $\epsilon_{D\infty} = 0$

Although no general closed-form expression for the DRT associated with conventional KWW frequency and time response is known for arbitrary β, an exact result for $H(x)$ for $\beta = 0.5$ is included in Ref. [41], and an expression for $G(\tau) = g_D(\tau)$ for the same β value was presented earlier [40]. It may be written in normalized form as

$$G(\tau) = (4\pi\tau\tau_o)^{-1/2} \exp(-\tau/4\tau_o). \tag{45}$$

Because this result is exact and because the $\beta = 0.5$ case of KWW response was explicitly considered by CTM [4], it will be used for illustrative purposes herein. Note especially that $G(\tau)$ diverges as $\tau \to 0$, while the associated $H(x)$ and $F(y)$ distributions do not. Although the above expression does not lead to a physically realizable response (as discussed in Appendix C, where it is modified to provide such response), it may nevertheless apply adequately over a wide frequency range and will be so used in this section. Thus, this expression was used in Eq. (34) to calculate the 'exact' $\beta = 0.5$ frequency response for the KWW model. Numerical quadrature using Romberg integration was set to yield an accuracy of at least nine decimal places.

Weighted, non-linear least squares procedures for the inversion of frequency-response data to estimate the elements of discrete distributions have been a part of the LEVM CNLS program for more than five years. Results of such estimation appear in Refs. [10,26,27,39,65]. Further, a new version of LEVM, V.7.0 (not commercially available until mid 1996, but used for the present work), incorporates means to estimate continuous (or discrete) distributions directly from either frequency *or* transient response data. The continuous distribution approach uses numerical quadrature, yields points on the $H(x)$ and $F(y)$ distributions denoted by $\{c_m, \tau_m\}$ or $\{c_m, y_m\}$, and is further described elsewhere [27]. For graphical presentation of results, the variable $s \equiv \log_{10}(x) = y \log_{10}(e)$ is more appropriate than y.

The CTM group [4], and recently Sarkar and Nicholson [58], have presented numerical tables of what they identify as g_m vs. s for the KWW distribution with $\beta = 0.5$. In spite of using different inversion methods, their results agree well. Unfortunately, however, as discussed in the last section, they both obtained *not* the g_m coefficients associated with $G(\tau) = g_D(\tau)$, but the dimensionless ones associated with $H(x)$ or $F(y)$ instead.

Since the weighted, non-linear least squares inversion methods for either temporal or frequency data included in the LEVM fitting program can yield estimates of both discrete coefficients, d_m, and of continuous-distribution ones, c_m, it seemed desirable to obtain these quantities for the $\beta = 0.5$ KWW situation using LEVM and 181 points of virtually exact KWW transient response data spanning the region $10^{-7} \leq t/\tau_o \leq 10^2$, with equal logarithmic intervals. Similar data were used by CTM and Sarkar and Nicholson. Note that while no $\epsilon_{D\infty}$ was included in the data generating model, effects of its inclusion are discussed below. To distinguish various inversion possibilities, it is helpful to introduce the letters 'D', 'C', 'F', and 'V' to designate the type of inversion

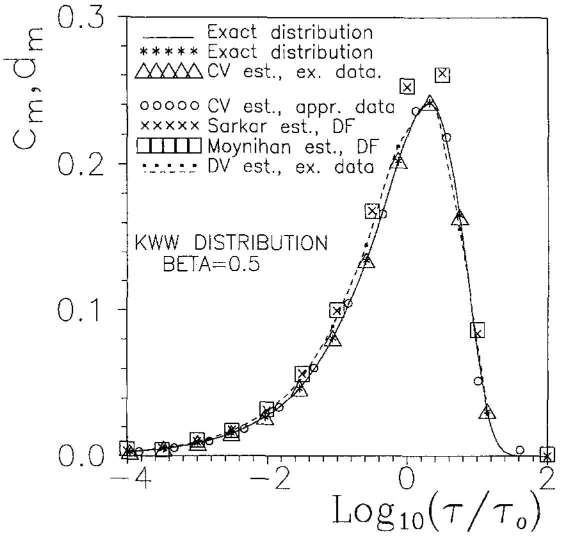

Fig. 1. Comparison of various inversion estimates of the $\beta = 0.5$ KWW continuous distribution of relaxation times, $\tau g_D(\tau)$, defined in Eqs. (36), (43) and (45). A list of acronym definitions is provided at the end of this work. The quantities d_m and c_m are estimated points on a discrete- or continuous-distribution, respectively. The solid line and asterisk points in the figure show the exact distribution behavior for $\beta = 0.5$. Sarkar and Moynihan used the DF inversion method, one which treats the distribution as discrete and employs fixed abscissa values, to invert exact transient data. Those fit results marked CV used an inversion method which is appropriate for a continuous distribution, one which also involves freely-variable abscissa fitting values. For one of these, the exact KWW transient-response data were inverted, and the other CV estimates show the results of inverting frequency-response data calculated from an approximate KWW model, one also appropriate for arbitrary β. The results denoted by triangles, squares, and crosses were obtained by inverting exact transient-response data, while those denoted by open and solid circles involved the inversion of frequency-response data. The CV inversion estimates shown by open triangles agree accurately with the exact distribution when the triangles evenly enclose the exact datapoints, denoted by asterisks. The KWW relaxation time, τ_o, is taken as 1 s here. The present inversions were carried out using exact transient and frequency-response data arising from the $\beta = 0.5$ KWW distribution alone, without any $\epsilon_{D\infty}$ contributions.

procedure used [27]. They denote discrete or continuous distributions fitted using a set of discrete independent-variable, τ_m, values held fixed (i.e., constant) during the inversion or all free to vary. Thus 'DF' denotes inversion involving a discrete-distribution approach with fixed τ values.

Fig. 1 shows the results of various inversions with $M = 19$. First, the d_m estimates of CTM and Sarkar and Nicholson are nearly indistinguishable in this graph. Were all the '×' symbols exactly centered in the open-square symbols, there would be no differences between them. The solid line in this graph was calculated from an $H(x)$ expression taken equal to τ times the $G(\tau)$ of Eq. (45). Because CTM and Sarkar and Nicholson obtained discrete-distribution estimates of a continuous distribution, their results are evidently not very accurate estimates of the exact distribution. But clearly their results approximate $H(x)$, rather than the $G(\tau)$ of Eq. (45). Further, a DF LEVM inversion of the transient data yielded results sufficiently close to those of these authors that they are not worth including separately in the graph. It should be noted that although DF inversion of transient data can be accomplished with linear least squares, such fitting usually leads to some non-physical negative d_m values, as in Ref. [4]. In the non-linear least squares LEVM approach, all d_m and c_m values are usually constrained to be positive but need not be.

The open triangular c_m points of Fig. 1 were obtained from a CV inversion of the time data using LEVM. The CV method is further described in [27], and results included therein suggest that frequency-domain CV inversion results for a continuous DRT may be of the order of ten times more accurate than CF ones, and both are appreciably superior to DV and DF estimates. The exact-distribution asterisk points shown in the figure were calculated from the exact distribution at the τ_m (or s_m) values obtained from the converged CV inversion. Thus, when the CV triangles surround the asterisk points evenly, their positions agree with the exact distribution, not only by falling on its line but by falling on it in the right places. Such agreement is excellent here, justifying the use of the CV inversion method as compared to a DF or DV approach.

The DV d_m estimated points on the dashed line included in the graph were calculated, using LEVM, from exact KWW frequency-response ($10^{-2} \leq \Omega_m \leq 10^7$) data. They are, of course, inferior to the CV temporal-inversion results but are superior to either DF or DV temporal-inversion results. Since 1987, a fitting model for generating approximate KWW frequency-response data [36] has been included in LEVM. It is applicable for the range $0.2 < \beta \leq 1$ and has been used with $\beta = 0.5$ to calculate such approximate response over the above frequency range. Then this data set was inverted using the CV approach, yielding the open-circle points shown in Fig. 1. Although the results are inferior to those obtained from the inversion of exact time or frequency-response data for, they are nevertheless far superior to those obtained by the DF approach.

Interesting and instructive as it may be to estimate DRTs associated with time or frequency response, the usual task in IS is to fit experimental data to one or more response models. Although LEVM allows one to fit with more than ten different continuous-distribution models, the lack of exact general expressions for KWW $G(\tau)$ and frequency response makes it difficult to fit data for arbitrary KWW β values. This lack was the reason for the development of the approximation method mentioned above [36]. CTM have used the DF method and tables derived from such inversion to provide a means to fit frequency-response data to the KWW model for arbitrary β. As shown above, it does not yield very accurate estimates of the $\beta = 0.5$ $H(x)$ or $F(y)$ response points. Nevertheless, because continuous-distribution frequency response is obtained as an integral over a distribution, as in Eqs. (34) or (36), errors in the estimates of the distribution points are partially averaged out in the calculated frequency response. It is of interest to quantify this expectation in order to evaluate and compare the utility of the two different methods of fitting KWW frequency-response data discussed above for $\beta = 0.5$.

Table 1 compares various standard-deviation fit measures, S_F, for fits of transient data, distribution estimates, and frequency-response data. The various different S_F quantities are defined in the table heading. The values listed in lines A and B in the table are the results of inverting exact KWW transient response to yield distribution estimates, while those presented in lines C and D were obtained by the direct inversion of KWW frequency-response data.

The estimated KWW distribution of lines A and B was used to calculate the associated frequency response, and the model for the exact response was fitted to it, yielding $\Delta\rho$ and τ_o parameter estimates and the estimated relative standard deviation of the fit, $S_{F\omega}$. Note that the S_{FDA} quantity, unlike the other standard deviation estimates, involves residuals rather than relative residuals. It therefore measures the degree of fit primarily in the region of the peak of the distribution, while all other S_Fs provide measures of the goodness of fit over the entire range of the dependent variable.

The extremely small value of S_{Ft} in line A of the table shows that the Eq. (42) DF model fits the KWW transient response data very well. The values of the two standard deviations in line A associated with the fit of the d_m coefficients to the exact $F(y_m)$ distribution, S_{FDA} and S_{FDP}, confirm the poor fit of the DF inversions shown in Fig. 1. The value of 1.4, for example, indicates an overall average error of fit of either sign of about 140%. But the corresponding frequency-response standard deviations are quite

Table 1
Standard deviations (SD) of fits of exact KWW data with $\beta = 0.5$; $M = 19$ used for inversion

	Fit type	Model	S_{Ft}	S_{FDA}	S_{FDP}	$S_{F\omega}$	
						Z	ϵ
A	t/DF	exact	7.1×10^{-5}	1.4×10^{-2}	1.4	1.8×10^{-4}	1.1×10^{-2}
B	t/CV	exact	1.2×10^{-6}	2.6×10^{-4}	3.6×10^{-3}	3.5×10^{-5}	1.1×10^{-4}
C	ω/CV	exact	–	3.5×10^{-4}	0.045	2.2×10^{-14}	3.0×10^{-8}
D	ω/CV	approx.	–	–	–	6.1×10^{-4}	2.3×10^{-2}

Lines A and B show results of inversion of exact transient-response data using proportional weighting, and lines C and D show results of CNLS inversion of exact frequency-response data with proportional weighting. Here, fit types t/DF and ω/CV indicate inversion of transient data (t) using the DF method or frequency-response data (ω) using the CV inversion method. See Appendix B for further definitions. S_{Ft} is the SD of the transient-fit relative residuals, the point-by-point differences between inversion fit values and the exact transient data, divided by the latter. S_{FDA} and S_{FDP}, in contrast, indicate the degree of agreement between predicted distribution values and exact values. S_{FDA} is the SD of the direct residuals, and S_{FDP} is that of the relative residuals. Finally, $S_{F\omega}$ is the SD of the relative residuals of the frequency-response data sets calculated from exact and estimated distributions. The ϵ-level results were obtained by transforming Z-level estimated frequency-response data to the ϵ-level and fitting the results with the exact (or approximate: line D) KWW response model at this level.

small, confirming the good degree of fit found originally for this case by CTM [4]. The first of the two $S_{F\omega}$ standard deviations is that for a CNLS frequency-response fit at the impedance level. The data and model values were then transformed to the complex dielectric constant level and fitting again carried out. As shown, the fit is far worse at this level even with the proportional weighting used for such fitting [24–27]. The parameter estimates for Z-level fitting were all excellent, generally within 0.1% or better of their exact values, but those obtained for epsilon-level fitting were appreciably worse. For example, that for τ_0 was 1.01 s, rather than its exact value of 1.0 s.

The line-B CV results are all much better than the DF ones and should be compared to the line-C ones. Here the exact Z-level frequency response was first calculated, and it was then inverted to yield the distribution estimate. Naturally, the accuracy of the direct Z-level fit results were limited only by round-off, but one again sees that transformation to the complex dielectric constant level before fitting to the original model leads to an inferior, but still excellent, fit. It is interesting to note that the distribution standard deviations of line C are inferior to those of line B, suggesting that the best estimates of the distribution for any appropriate β value should be obtained by inverting Eq. (35) rather than Eq. (36), at least for exact discrete data.

Finally, line D shows results of fitting the approximate KWW model in LEVM to exact $\beta = 0.5$ frequency response. Let a quantity written as $P|Q$ indicate the estimate of the quantity, P, and its estimated relative standard deviation, Q. The raw parameter estimates obtained for the two levels for, $\Delta\rho$, τ_0 and β were, respectively, $1.0004|8 \times 10^{-5}$, $0.996|7 \times 10^{-4}$, and $0.4965|4 \times 10^{-4}$ for Z-level fitting and $1.0000|10^{-9}$, $1.014|6 \times 10^{-3}$, and $0.5243|3 \times 10^{-3}$ for epsilon-level fitting. Within its range of applicability, the approximate KWW fitting model yields Z-level parameter estimates with errors of the order of 1% [36], but their accuracy can usually be somewhat improved by an interpolation method. For example, this method changes the above value of 0.4965 to 0.5004, much closer to the exact value.

The above results provide some basis for comparing the strengths of the various methods one can use to fit KWW data with an unknown β to a KWW model. The CTM method [4] apparently uses mostly graphical and tabular values to obtain estimates of the three relevant parameters. It is therefore a small-number-of-points fitting method and may be expected to yield rather poor estimates (see example presented in the next section), even if it were based on CV rather than DF inversion. Clearly, a better alternative is to fit using the LEVM approximate model [36]. For most data, those with errors of the order of a few percent or more, this approach should be preferred.

On the other hand, if the data appeared particularly good and one wanted to obtain more accurate parameter estimates, one could use an iterative method. Initial parameter estimates obtained from fitting with the approximate method could be used to calculate, as discussed below, the associated KWW transient response and then the CV $\{c_m, y_m\}$ distribution estimates. These could then be used to obtain the associated frequency response and that then compared with the original data. Fitting of this calculated frequency response data with the approximate model would then yield new parameter estimates, and the process could be continued until, hopefully, sufficient convergence was obtained. An alternate approach might again start with the experimental frequency-response data and obtain the associated DRT and transient response data. The latter could then be fitted by the exact KWW transient response function to obtain new parameter estimates. But it should be noted that the larger the error in the original data, the smaller the number of significant c_m estimates that can be obtained. Thus, for most KWW fitting situations, the approximate KWW model should be used and its adequacy compared with results obtained from fitting with other reasonable models such as that of Cole and Davidson [66].

7.2. $\epsilon_{D\infty} = 10$

There is a problem in implementing the fitting possibilities mentioned above. When one contemplates using any of Eqs. (33)–(36) with experimental data in order to estimate a DRT such as $H(x)$, it must be recognized that the data will always involve a contribution from $\epsilon_{D\infty}$. It is then improper to use full $\hat{Z}(\omega)$ or $\hat{M}(\omega)$ data directly with any of these equations. If one does so, the $H(x)$ DRT obtained from a CV inversion of the data will include the effect of $\epsilon_{D\infty}$ and will thus not represent only the DRT of the actual response model. Instead, one must represent the response associated with $\epsilon_{D\infty}$ separately so as not to confound its effect with that of the actual proper DRT [27]. The general situation is illustrated in Fig. 2, which shows how the effects of CSD, DSD, and electrode and wiring contributions can be combined into an overall equivalent circuit. In the present situation, the DSD dispersion element, DED, should be omitted; C_∞ is $C_{D\infty}$; the CSD dispersion element, DEC, represents $\Delta RI(\omega)$ at the Z-level; and electrode effects will be discussed later.

To illustrate the problem, let us generate synthetic impedance-level frequency-response data with no electrode-polarization contribution; with $\epsilon_{D\infty} = 10$ and $\rho_{C\infty} = 0$; with the DEC entity taken as the DSD KWW frequency-response model, $I(\omega)$ times $\Delta\rho$ for $\beta = 0.5$ and $\tau_o = 1$ s; and with a value $\Delta\rho = 1/\sigma_0$ determined from the CTM Eq. (1). Then take $\langle x \rangle_D = 2$, so $\Delta\rho = 2.2588495 \times 10^{12}$ Ω cm. For such data, it follows that $\epsilon_{C\infty} = 10$.

This data set, extending from $\Omega = 10^{-4}$ to 10^6 with equal logarithmic intervals, was then used for two separate CV inversions with $M = 19$. Results are shown in Fig. 3 with a log–log presentation, one which better illustrates the degree of fit in the tails of the distribution than does that of Fig. 1. In the first inversion, the DRT set $\{c_m, \tau_m\}$ was determined with the C_∞ of Fig. 2 included as a separate fitting parameter of the complete model. It led to the points denoted by open triangles in the log–log plot of Fig. 3. These results represent the true DRT curve nearly

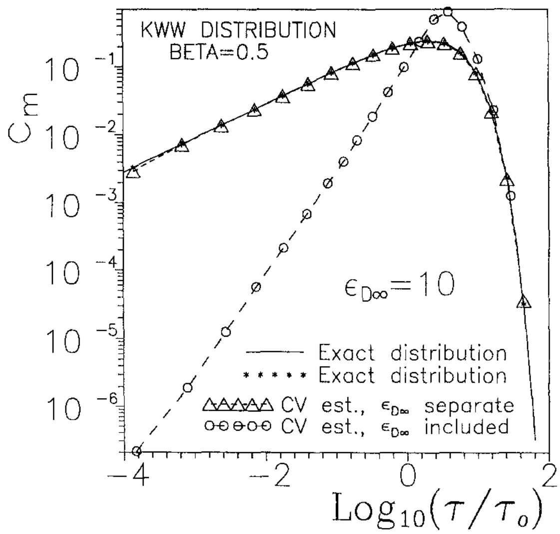

Fig. 3. Log–log plots of CV inversions of exact $\beta = 0.5$ KWW frequency-response data which also involved the presence of an $\epsilon_{D\infty}$ value of 10. The c_ms are estimated points of the continuous KWW distribution. The solid-line distribution curve, involving open triangular points, where $\epsilon_{D\infty}$ was treated separately from the DRT itself, as in Fig. 2, agrees very closely with the corresponding one of Fig. 1 for which no $\epsilon_{D\infty}$ was present. The dashed curve was derived by inverting the data without separate account of $\epsilon_{D\infty}$. Thus the effects $\epsilon_{D\infty}$ of are included in the derived DRT, yielding an inappropriate estimate of it.

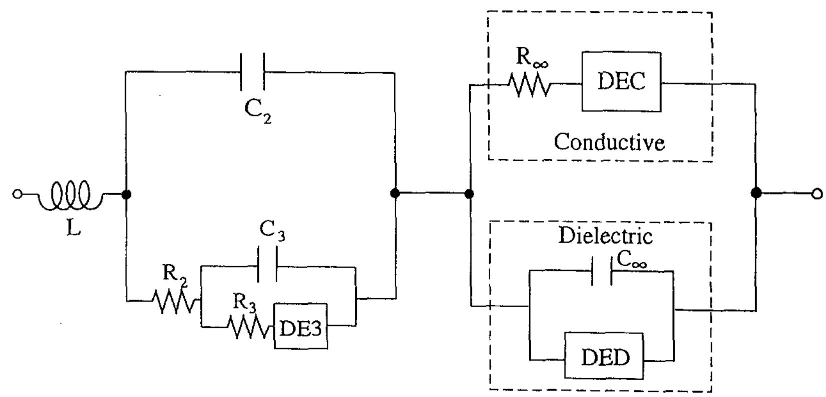

Fig. 2. An equivalent circuit implemented in LEVM for fitting small-signal ac frequency-response data. Here 'DE' denotes a distributed circuit element, one which cannot be represented by a finite number of ideal circuit elements; 'C' denotes conductive response, and 'D' dielectric response. Thus, the element marked DEC (dispersive element, conductive) designates conductive-system dispersion (CSD). In actual situations, some of the circuit elements shown may be unnecessary. For $\epsilon_{D\infty} \neq 0$, $C_\infty \equiv C_{D\infty}$ must be taken non-zero.

as accurately as those shown in Fig. 1, except for slight deviations at the endpoints. When these were omitted, the S_{FDA} and S_{FDP} values were 3.2×10^{-4} and 0.033.

The second inversion did not include C_∞ separately in the fitting model, so its effect thus became melded into the DRT estimate. It led to the curve denoted by the dashed line and open circles. This curve shows a left-side slope of 1.5 rather than the 0.5 of the proper KWW DRT. For the first fit, the $\epsilon_{D\infty}$ estimate was 10.004 ± 0.003, and the estimated $\langle x \rangle_D$ and $\langle x^2 \rangle_D$ values were 1.9992 and 11.997, very close to the correct values of 2 and 12. For continuous data with $x_{min} = 0$, $\langle x^{-1} \rangle_D$ and $\langle x^{-2} \rangle_D$ should be infinite, but with the limited span of the present data, their estimates were large but finite. The estimates of $\langle x \rangle_D$ and $\langle x^2 \rangle_D$ for the second inversion were 4.00003 and 23.9995. The above values for the fit with $\epsilon_{D\infty}$ separate and not included

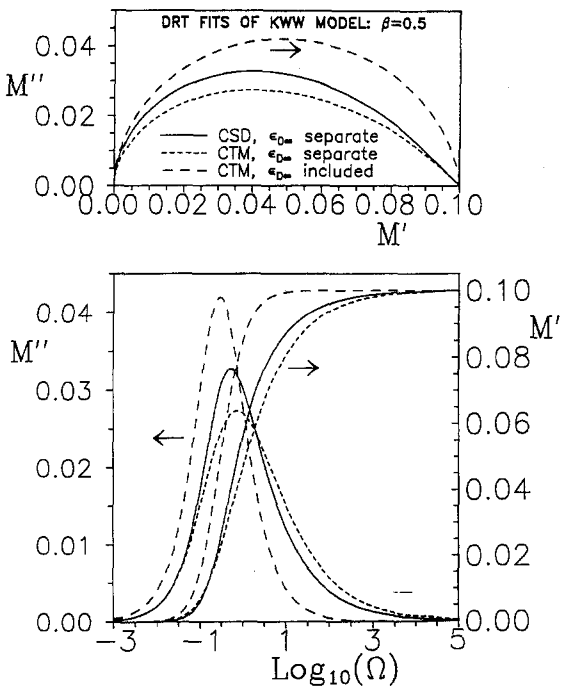

Fig. 4. Complex-plane and frequency-response curves of $M(\Omega)$ obtained by CNLS fitting of exact data calculated using the KWW DRT and $\epsilon_{D\infty}$ as in Table 2 and Fig. 3. The CSD and CTM designations (see acronym listing) refer, respectively, to the disparate KWW fitting approaches defined by Eqs. (38) and (37) (as corrected in Appendix A, both with the KWW $G(\tau)$ of Eq. (45), and both using Eq. (39). Here $\Omega \equiv \omega\tau_0$ and $\tau_0 = 1$ s.

in the DRT yield $\epsilon_{C0} \simeq 10$ from Eq. (16). Similarly, the CTM Eq. (3) leads to $\epsilon_{C0} \approx 20$ and 5, for $\epsilon_{D\infty}$ not included in the DRT estimate and included in it, respectively.

Complex-plane and frequency-response results of the two separate inversions of the same data set are shown graphically in Figs. 4–7 for the four immittance levels. To produce these results, the CV $\{c_m, \tau_m\}$ DRT sets obtained from the two separate inversions were used with CV quadrature to obtain separate estimates of $I(\Omega)$. These estimates were used in Eqs. (38) and (39) to obtain the proper CSD results, which agree with the original p-level data very closely, and were then used in Eq. (37) to calculate CTM predictions. Comparisons of the three different response curves at each of the four levels are instructive. Because the DRT in which the effects of $\epsilon_{D\infty}$ are included is so different from the proper one, it is not surprising that its results differ as much as they do from the results obtained by using a close estimate of the exact DRT used in generating the data. In the log–log plots of Fig. 6, the lower $\sigma'(\Omega)$ curves show $\sigma'(\Omega) - \sigma_0$ response, and so they approach limiting slopes of 2, consistent with Eq. (12). Fig. 7 demonstrates that the values of ϵ_{C0} calculated above are consistent with the ϵ_0 values shown. The differences between the CSD and CTM fit curves are most extreme at the dielectric level.

7.3. CSD and CTM direct data fits with different $\epsilon_{D\infty}$ values

Although the results of Sections 7.1. and 7.2. demonstrate clearly the effects of proper and improper treatment of $\epsilon_{D\infty}$ in inversion, they deal only with a DSD data situation, not particularly appropriate for the original or even the corrected CTM frequency-analysis approach. Therefore, it is important to compare the CSD and CTM fitting results for exact CSD data (see Appendix A for further details). Two exact Class-A KWW data sets with $\beta = 0.5$ and $\epsilon_{D\infty} = 10$ ad 2 were therefore prepared and were fitted with the Class-B approximate KWW model of LEVM, including the effect of an $\epsilon_{D\infty}$ as a free parameter of the fitting circuit. The results of these fits are shown in Tables 2 and 3.

For the present fits, the CSD results using PWT are comparable to the CTM ones with unity weight-

Table 2
Results of CNLS fitting with proportional or unity weighting of synthetic CSD KWW frequency-response data involving a value of $\epsilon_{D\infty}$ of 10 and $\beta = 0.5$

Fit method	A Exact	B CSD/PWT	C CTM/PWT	D CTM/UWT
S_F	–	0.027	0.22	–
ϵ_∞	20	19.84|0.0003	18.68	20.01
τ_0 (s)	1	2.05|0.008	0.439|0.23	0.983|0.028
β	0.5	0.4951|0.002	0.5201|0.02	0.4982|0.004
$10^{-12}\rho_0$ (Ω cm)	2.2589	2.212|0.003	1.744	2.503
$\langle\tau\rangle$ (s)	6	4.18	0.819	1.98
ϵ_{C0}	30	30.22	15.82	29.78
ϵ_0	40	40.22	25.87	40.08

The notation $P|Q$ used herein and later indicates the estimate of the quantity, P, and its estimated relative SD, Q; values without SD estimates are calculated. Here and elsewhere, S_F is the relative SD of residuals formed by taking the differences between frequency-response points obtained by fitting and corresponding exact data values. ϵ_∞ is the high-frequency-limiting value of $\epsilon'(\omega)$. τ_0 is the relaxation time in the KWW transient response expression, and β is its fractional exponent. ρ_0 is the DC resistivity, and $\langle\tau\rangle$ is the first moment, or average, of τ over the KWW distribution (seeAppendix A). Finally, ϵ_{C0} is the zero-frequency limiting value of ϵ arising from CSD, and here $\epsilon_0 = \epsilon_{C0} + \epsilon_{D\infty}$ since no DSD is present.

ing (UWT). The large S_F values in the CTM/PWT columns arise from the inaccuracy in the approximate KWW model at low frequencies (see Appendix A), a region which plays much less of a role in UWT fitting at the modulus level. With a model involving accurate response in the low-frequency region, it would be preferable to use PWT. For the calculation required for these tables, the values of needed $\langle x^m \rangle$ quantities associated with each β estimate were used [41], and the CTM ρ_0 figures are extrapolated values. Further, known values of $\epsilon_{D\infty}$ were used as needed. For the Table 2 fit, where exact $\epsilon_{D\infty}$ and $\epsilon_{C\infty}$ values were each 10, estimated values of these quantities for Cols. C and D were 12.91|0.08, 5.77|0.19 and 10.10|0.02, 9.91|0.02, respectively. The exact values for Table 3 were 2 and 10; no separate estimates of them could be obtained for the CTM/PWT fit, but the CTM/UWT estimates were 2.18|0.05 and 9.83|0.01, respectively.

8. Detailed analysis of the relaxation frequency response of a model glass

Finally, it is worthwhile to apply some of the results discussed above to the analysis of experimental data for a conducting system showing dispersion.

Table 3
Results of CNLS fitting with proportional or unity weighting of synthetic CSD KWW frequency-response data including a value of $\epsilon_{D\infty}$ of 2 and $\beta = 0.5$

Fit method	A Exact	B CSD/PWT	C CTM/PWT	D CTM/UWT
S_F	–	0.030	0.246	–
ϵ_∞	12	11.92|0.003	11.18|0.02	12.01
τ_0(s)	1	2.01|0.008	0.955|0.03	0.970|0.02
β	0.5	0.4965|0.002	0.5635|0.008	0.4962|0.002
$10^{-12}\rho_0$ (Ω cm)	2.2589	2.211|0.003	1.671	2.511
$\langle\tau\rangle$ (s)	6	4.08	1.57	1.967
ϵ_{C0}	30	30.24	29.2	30.03
ϵ_0	32	32.24	31.2	32.03

See footnote of Table 2 for further information.

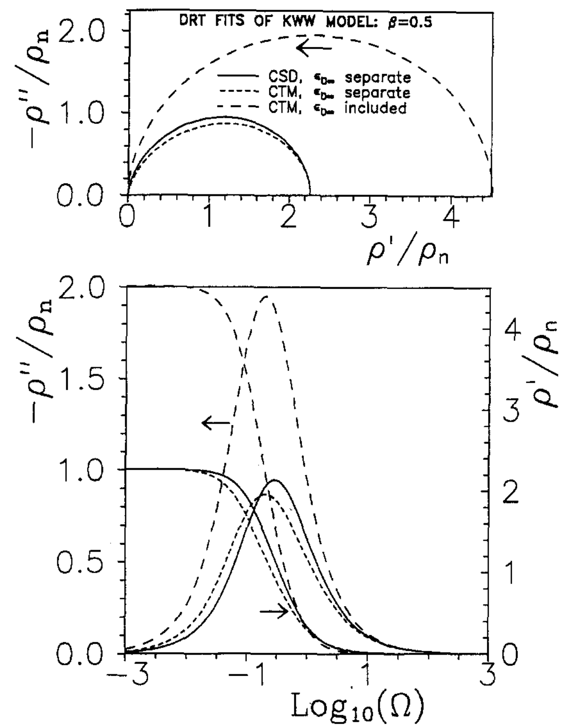

Fig. 5. Complex-plane and frequency-response curves of the normalized complex resistivity, $\rho(\Omega)/\rho_n$. See the caption of Fig. 4 for definitions. Here, $\rho_n = 10^{12}\,\Omega$ cm.

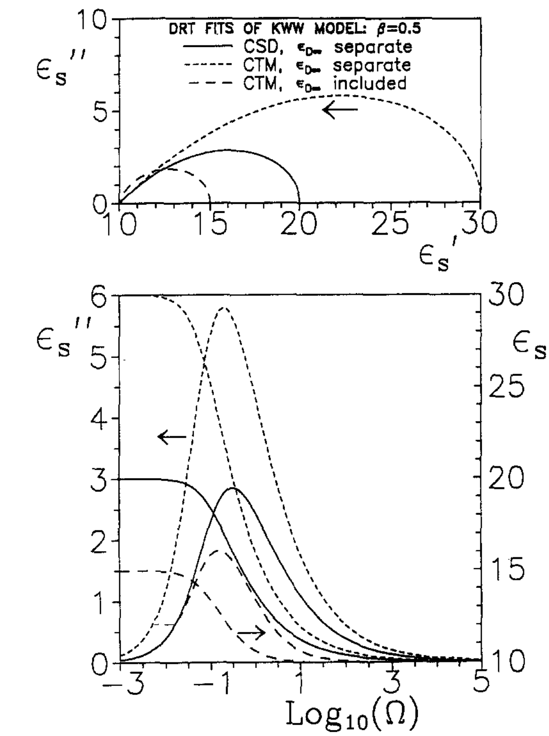

Fig. 7. Complex-plane and frequency-response curves of $\epsilon_s(\Omega) \equiv \epsilon(\Omega) - \sigma_0 / i\omega\epsilon_V$. See the caption of Fig. 4 for definitions.

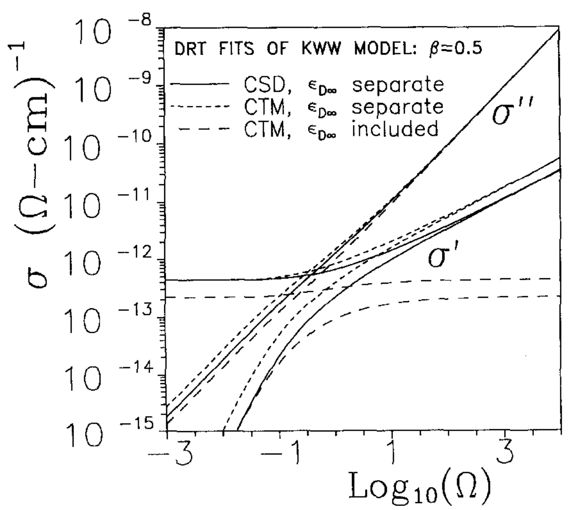

Fig. 6. Log–log frequency-response curves of $\sigma(\Omega)$. See the caption of Fig. 4 for definitions. The σ' curves which approach the x-axis are for $\sigma_s' \equiv \sigma'(\Omega) - \sigma_0$.

Recently, Moynihan [32] has re-analyzed the relaxation data for a typical ionically conducting glass, that of $Li_2O–Al_2O_3–2SiO_2$ (LAS) at 24.0°C. These data were first considered in Refs. [1,4] and have also been analyzed by others since then (e.g., [54,67]). According to Moynihan, they exhibit one of the broadest distributions of relaxation times found for such materials. Here I shall follow Moynihan and primarily consider fitting of KWW and Cole–Davidson (CD) models. The data themselves were kindly provided by Dr Moynihan [68]. CNLS fitting was carried out with proportional weighting of a circuit involving the approximate KWW response element of LEVM or another $I(\omega)$ response model.

The empirical response function introduced by Havriliak and Negami [69] is

$$I(\Omega) = \left[1 + (i\Omega)^{\psi}\right]^{-\gamma}, \tag{46}$$

where $0 < \psi, \psi\gamma \leq 1$. When $\gamma = 1$, it reduces to Cole–Cole response, and for $\psi = 1$ it yields Cole–Davidson behavior. Here $\Omega \equiv \omega\tau_0$ as usual. The Cole–Cole form of Eq. (46), originally introduced to describe dielectric dispersion, was perhaps first introduced at the Z-level in 1957 by Schwan [70] (see pp. 160–161), and it and the general Eq. (46) function are now widely used for fitting CSD response [11]. The CD form was first used in the context of the CTM fitting method in 1977 [54].

It is worthwhile to compare fitting results for these data using the CTM and CSD fitting methods. The A, B, and C columns of Table 4 show results of fitting with the CTM method. Column A summarizes parameter estimates obtained from the recent Moynihan KWW fitting using graphical and tabular methods [32]. These parameter values should be compared to those in Col. B obtained with full CNLS fitting of the data at the M- (or ρ-) level. Initial CNLS fitting of the data without any account of electrode polarization effects led to very poor results, with S_F values for the KWW and CD fits of greater than 0.2. Such poor fits are inconsistent with the statements in Refs. [3,54] that large electrode capacitances need not interfere with analysis of relaxation data using the CTM M-level formalism. The reason is that with CNLS fitting using proportional weighting the results of ρ-level and M-level fitting are exactly the same, and although low-frequency polarization behavior appears obscured in $M''(\omega)$ plots, its role in CNLS fitting is not reduced by transformation from the Z- to the M-level. Incidentally, in none of the fits presented in Table 4 was a statistically significant estimate of $\rho_{C\infty}$ different from zero obtained.

Clearly, to obtain a useful CNLS fit of these data, one must add response elements to account for electrode polarization and any other interfacial effects. It has been found that the combination of the capacitance C_2 and a specific form of the DE3 distributed element of Fig. 2 does so very well when DE3 is taken as a constant-phase element, a common choice for representing such behavior [11,71]. The resulting electrode response may be written at the complex conductivity level as

$$\sigma_E(\omega) = i\omega\epsilon_V\epsilon_E + A_E^{-1}(i\omega)^{n_E}, \quad (47)$$

where $0 < n_E \le 1$, ϵ_E is a dielectric constant associated with the electrode capacitance, and A_E is independent of frequency. Note that the corresponding $\rho_E(\omega)$ response is in series with the bulk response, as shown in Fig. 2. Although inclusion of a non-zero

Table 4
Results of CNLS fitting with proportional weighting of 24°C $Li_2O–Al_2O_3–2SiO_2$ frequency-response data by CTM and CSD fitting methods using approximate KWW and exact CD response models

Method, model	A CTM, KWW	B CTM, KWW	C CTM, CD	D CSD, KWW	E CSD, KWW	F CSD, KWW	G CSD, CD
S_F	–	0.066	0.050	0.028	0.016	0.034	0.041
ϵ_∞	8.475	9.29|0.021	8.44|0.015	9.04|0.005	9.42|0.005	9.43|0.005	10.3|0.011
$10^{-9}\rho_0$ (Ω cm)	1.098	1.019	0.997	1.089|0.005	1.076|0.003	1.075|0.006	1.068|0.008
$10^3\tau_o$ (s)	0.365	0.36|0.044	2.77|0.041	1.197|0.016	1.105|0.013	1.095|0.014	4.25|0.048
β or γ	0.47	0.468|0.027	0.269|0.035	0.5586|0.008	0.5354|0.007	0.5347|0.005	0.375|0.027
$10^{-8}A_E$	–	1.77|2.1	11.7|0.5	1.23|0.22	1.21|0.013	–	1.31|0.028
n_E	–	0.643|0.175	0.810|0.038	0.636|0.004	0.526|0.014	–	0.463|0.017
ϵ_E	–	–	–	–	74.8|0.027	–	50.0|0.047
$\langle x\rangle_D$	2.257	2.277	0.269	1.663	1.776	1.780	0.375
$\langle x^2\rangle_D/(\langle x\rangle_D)^2$	3.484	3.522	–	2.354	2.201	2.207	–
$10^3\langle\tau\rangle_D$ (s)	0.82	0.82	0.745	1.991	1.963	1.949	1.59
ϵ_{C0}	29.5	32.7	–	30.9	31.6	31.5	27.1
ϵ_0	29.5	32.7	–	30.9	31.6	31.5	27.1

The A_E, n_E, and ϵ_E parameters account for electrode polarization effects; see the heading of Table 2 for other definitions. Column-A parameter estimates are those of Moynihan [32], obtained largely by graphical and tabular methods. All other results were obtained by full CNLS fitting. Some otherwise comparable fits include two or three electrode parameters while others do not. For the fits of Cols. B and C, only two such parameters are included because the results better agreed with those of Col. A. The electrode parameter ϵ_E was omitted from the Col.-D fit to allow direct comparison with the results shown in Col. E, where it was included. The estimates shown in Col. F were obtained by first using LEVM to eliminate estimated electrode effects from the Col.-E fit data predictions and then refitting the results without electrode parameters included.

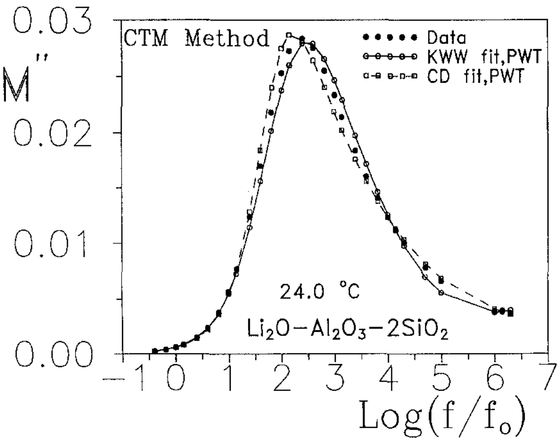

Fig. 8. Plots of M'' vs. $\log(f/f_0)$ for LAS glass at 24°C. Lines and open-symbol points show KWW and CD CNLS fits to the data using the corrected CTM approach. Here and subsequently, 'KWW fit' denotes the use of the approximate KWW-model algorithm of the LEVM CNLS fitting program; PWT stands for proportional weighting; and $f_0 = 1$ Hz. The estimated fit parameters of the KWW and CD fits are listed in Table 4, Cols. B and C, respectively.

value of ϵ_E leads to smaller S_F values than shown, the fits of Cols. B and C were carried out without this element, since the results obtained were closer to those shown in Col. A and that quoted in Ref. [54]. In fact, most of the common Col.-A and Col.-B results are quite close, except for those of $\epsilon_{D\infty}$ and ϵ_{C0}. The only parameter value available from prior CD fits of these data is that of γ, 0.26 [32] and 0.262 [54]. Fig. 8 compares M'' data with the Cols. B and C KWW and CD model fits. These CTM-approach fit results appear close to those presented earlier [32,54], but it is clear that neither model leads to an adequate fit of the data.

Columns D–G of Table 4 list the results of CSD fits of these data. Those of Col. D should be compared with the values in Col. B. Note not only the differences in the corresponding parameter estimates but also the much smaller values of the Col. D S_F and parameter relative standard deviation estimates. Especially noteworthy are the differences between τ_0 and $\langle x \rangle_D$ values.

The fit of Col. E included a non-zero ϵ_E and it is clear that its presence greatly improves the fit but does not appreciably change the estimates of most of the bulk parameters. By contrast, the use of a non-zero ϵ_E with no added constant-phase element yielded a very poor fit. One can use LEVM to eliminate the effect of any fitting parameters from the data. The fit results of Col. F are for fitting of data from which the effects of the electrode-polarization parameters of Col. E were so eliminated. The parameter estimates are virtually identical to those of Col. E, but the S_F value is larger because of the magnification of data errors arising from subtraction.

In addition to the KWW and CD model fitting results of Table 4, the usefulness of several other fitting models available in LEVM was also investigated. Of these CSD fits, only two other models led to S_F values comparable to that of the Col.-E fit of Table 4. The full Havriliak–Negami model yielded a S_F value of 0.0216 and the general exponential distribution of activation energies model [7] led to 0.0177, nearly as good as the value following from the present approximate KWW model.

All the CNLS fit results in Table 4 are for the Class-B type of dispersion models discussed in Appendix A. There, it is shown that fitting with Class-A models leads to more complete and accurate results than fitting with Class-B models. Thus, it is worthwhile to present a few results with Class-A model fitting using PWT, especially since they may help separate the $\epsilon_{C\infty}$ and $\epsilon_{D\infty}$ contributions to ϵ_∞. The Col.-F data were therefore first fitted with an exponential-distribution-of-activation-energies model [6,9]. The fit yielded a zero estimate of the separate $\epsilon_{D\infty}$ fitting parameter and an estimate of $\epsilon_{C\infty}$ of 9.41, close to that for ϵ_∞ in Col. F. Then the same data were fitted with the $\beta = 0.5$ exact KWW model, even though the β estimate shown in Col. F is somewhat larger than 0.5. Again, a zero estimate of $\epsilon_{D\infty}$ was obtained, along with an $\epsilon_{C\infty}$ estimate of 9.35. The KWW fit involved a 20% larger S_F value than did the exponential-distribution one, probably mostly because of the β mismatch arising from the restriction to $\beta = 0.5$. Finally, the data were fitted with the approximate KWW model using the CTM approach with UWT. Although an estimate of $\epsilon_{D\infty}$ of 1.12|0.63 was obtained, the value seems too small and the relative standard deviation too large to allow meaningful conclusions to be reached. The two Class-A $\epsilon_{C\infty}$ estimates and the inability to obtain significant non-zero $\epsilon_{D\infty}$ estimates strongly suggest that the CSD-approach Class-B ϵ_∞ estimates shown in the table are dominated by $\epsilon_{C\infty}$ and justify the

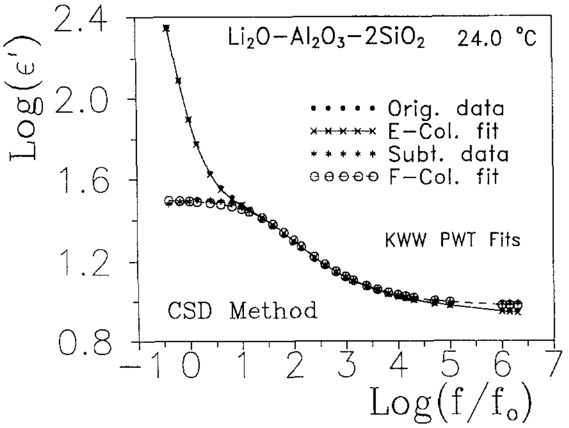

Fig. 9. Log–log plots of ϵ' vs. frequency for a CSD-method, KWW-model fit which includes both bulk and electrode contributions to the fitting model, and for a fit to data from which the electrode contributions determined in the first fit were subtracted. See Table 4, Cols. E and F, respectively.

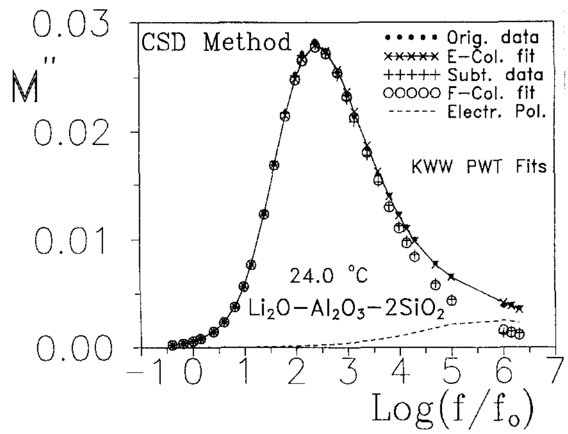

Fig. 10. Plot of M'' for a CSD-method fit to the original data set and a fit to that with the electrode contribution subtracted. See Table 4, Cols. E and F, respectively. The dashed line shows the electrode polarization contribution that was subtracted.

neglect of $\epsilon_{D\infty}$ in the calculations of ϵ_{C0} and ϵ_0 presented in the table.

It is interesting to compare some normalized frequencies associated with the Col.-F fit results. Let $\Omega_x \equiv \omega_x \tau_o = (\tau_x/\tau_o)^{-1}$ and take τ_x as $\langle \tau \rangle_D$, $\tau_{\rho p}$, τ_{Mp}, and $\tau_{\epsilon p}$ where the 'p' subscript denotes the value of ω at the peaks of the $\rho''(\omega)$, $M''(\omega)$ and $\epsilon_s''(\omega)$ curves. Then one finds for Ω_x: 0.615, 0.392, 1.75, and 0.289, respectively. Thus, for the present data, the peak of the M'' curve appears at a frequency about 6 times greater than that of the ϵ'' curve. For comparison with the Col.-F value of $\langle x \rangle_D$, calculated from the estimated value of β listed, an $M = 7$ DRT inversion of the present data, where $\epsilon_{D\infty}$ was accounted for separately, led to an estimate of this quantity of about 1.88. The difference between the two values probably arises from the use of the approximate Class-B KWW model, from a relatively small value of M, and from errors in the data.

The three CSD KWW fits of Table 4 yield mutually consistent estimates of ϵ_{C0} and ϵ_0, ones better than the others listed in the table. Fig. 9 shows a log–log plot comparing the frequency dependence of the original $\hat{\epsilon}'$ data with that predicted from the Col.-E fit, and a comparison of the data with electrode polarization effects subtracted from it with the Col.-F fit results. It is clear that polarization makes a non-negligible contribution to the total response at both the low-frequency and the high-frequency ends of these curves. Figs. 10 and 11 show similar results for M'' and M' and include curves showing the separate contributions from electrode polarization as well. The high-frequency polarization effects present here are associated with the semi-blocking response of the electrodes. This response may arise from the use of non-parent-ion electrodes. It seems likely that such polarization effects together with the use of more appropriate fitting methods may explain much

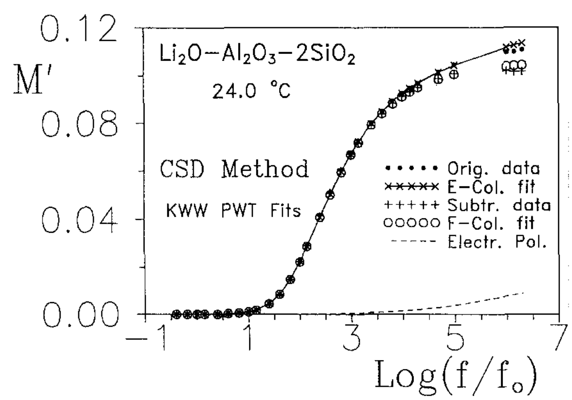

Fig. 11. Plot of M' for a CSD fit to the original data set and a fit to that with the electrode contribution subtracted. See Table 4, Cols. E and F, respectively. The dashed line shows the electrode polarization contribution that was subtracted.

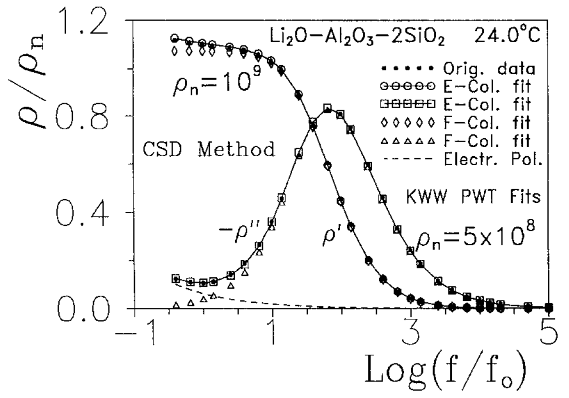

Fig. 12. Plot of ρ'/ρ_n and ρ''/ρ_n CSD fit results to the original data set and to that with the electrode contribution subtracted. See Table 4, Cols. E and F, respectively. The dashed line shows the electrode polarization contribution that was subtracted. Here for clarity the ρ''/ρ_n results are magnified by a factor of two compared to the ρ'/ρ_n ones. The units of ρ_n are Ω cm.

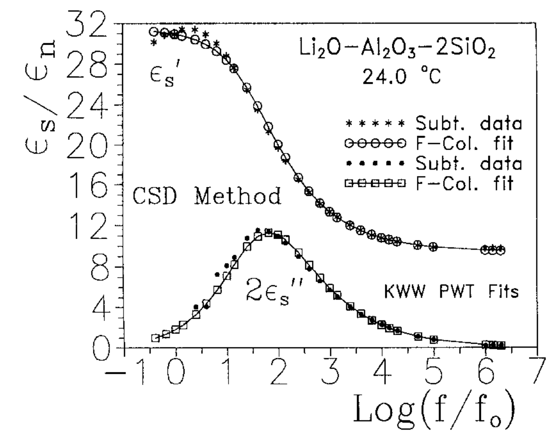

Fig. 14. Plot of ϵ_s/ϵ_n CSD fit results to the original data set and to that with the electrode contribution subtracted. See Table 4, Cols. E and F, respectively. Here $\epsilon_n = 1$ for the real part and 0.5 for the imaginary part of ϵ_s; $\epsilon_s(\Omega) \equiv \epsilon(\Omega) - \sigma_0/i\omega\epsilon_v$; and $\Omega \equiv \omega\tau_o$.

of the excess high-frequency absorption that CTM [4] have termed "endemic to the vitreous state".

Fig. 12 presents ρ' and ρ'' response comparisons and shows that, for these ρ-level plots, electrode effects only make significant contributions at low frequencies. Here the polarization curve is only shown for ρ'' response. Fig. 13 is similar to Fig. 6 but, again, makes it clear that electrode polarization contributes significantly to the data at both low and high frequencies. Note especially the reduction in the

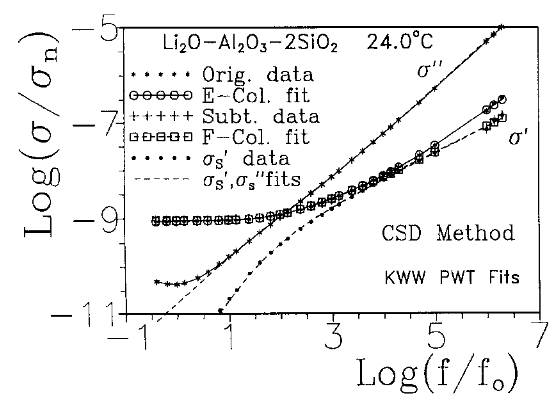

Fig. 13. Log–log frequency-response curves of $\sigma(\Omega)/\sigma_n$ CSD fits to the original data set and to that with the electrode contribution subtracted. See Table 4, Cols. E and F, respectively. The σ' curve which approaches the x-axis is that for $(\sigma'(\Omega) - \sigma_0)/\sigma_n$; $\Omega \equiv \omega\tau_o$; and here $\sigma_n = 1\ (\Omega\ \mathrm{cm})^{-1}$

slope of the original log–log σ' vs. f frequency-response curve, which reaches a maximum exceeding 0.75 at the highest measured frequencies, to a constant slope near 0.5 over a wide frequency range for the subtracted data and fit. The KWW model without any polarization contributions thus fits the subtracted data much better over a wide frequency span. The excellent agreement between data and CSD fit results shown in Figs. 9–13 is much superior to earlier fitting results of others. The present fit results strongly indicate that the approximate KWW model is appropriate for these data. At most only slight deviations between data and fit appear at the extremes of frequency.

Fig. 14 shows the dependences of the real and imaginary parts of ϵ_s on frequency, with the imaginary part expanded by a factor of 2 for clarity. It is important to emphasize that while the ϵ_s' curve involves data from which the electrode polarization contribution has been subtracted, the ϵ_s'' data and fit curve also involve the additional subtraction of the estimated σ_0 value. At low frequencies, the subtracted ϵ-level quantities are nearly equal, greatly magnifying the errors in the original data. Thus we see a small reduction in the ϵ_s' data at the lowest frequencies, and much more disagreement between data and fit for ϵ_s'' in this range. The four lowest ϵ_s''

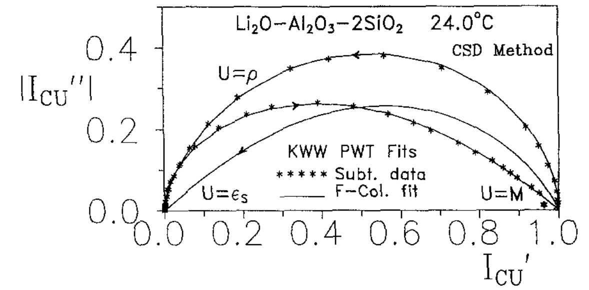

Fig. 15. Complex-plane data and CSD fits to the data with electrode contribution subtracted. The normalized quantity $I_{CU} \equiv (U - U_\infty)/(U_0 - U_\infty)$, where U is ρ, M, or ϵ_s, and $\epsilon_s(\Omega) \equiv \epsilon(\Omega) - \sigma_0/i\omega\epsilon_V$.

data values were so noisy that they have been omitted. The final low-frequency-limiting value of ϵ_s' from the fit is 31.474 here, the same as that shown in Col. F of Table 4. Note that these ϵ_s results were not obtained by direct DSD fitting of the data at the epsilon or complex conductivity level but follow from the transformation of the Col.-F ρ-level CSD fits and data to the epsilon level.

Fig. 15 shows complex-plane plots of the ρ, M, and ϵ_s fits and data, all normalized to afford easy comparison. Because of the large amount of noise in the low-frequency ϵ_s'' data, the ϵ_s curve shown is that for the Col-F fit only. It is interesting to note that for the present data, the M and ϵ_s curves are nearly mirror images of each other, a consequence of β being near 0.5 for these data.

The subtraction of the electrode polarization effects from the full data is particularly easy with CNLS fitting because the electrode and bulk effects are in series, as in Fig. 2. The remaining bulk data and its separate fitting, as in Col. F, show extremely plausible behavior here, strongly justifying the identification of the series fitting parameters with electrode processes. Since such parameters should be intensive and thus independent of electrode spacing, it is nevertheless always desirable to make measurements on samples of two or more thicknesses, allowing unambiguous identification of bulk and electrode effects.

The Fig. 15 results again raise the question of identification mentioned in Section 4: do the data arise from DSD with a separate σ_0 or from CSD with a separate $\epsilon_{D\infty}$? Although it may be possible, as discussed in Section 4, to discriminate on the basis of different temperature dependences, other means of identification would be welcome as well. The results of the following three tests seem to provide another such method. First, a CSD complex data set was formed using the CD response model with $\gamma = 0.6$ and $\epsilon_{D\infty} = 10$. These exact ρ-level data values were converted to the complex σ level and the effects of σ_0 then subtracted. These subtracted-data were then converted to the complex ϵ-level and fitted to a response model which included CD response at the dielectric level and $\epsilon_{D\infty}$, thus representing full DSD response. The second test was similar but started with ρ-level data containing 2% random errors drawn from a normal distribution having zero mean. The third test was also similar but involved fitting and analysis of the actual Col.-F LAS-glass data set.

All three tests described above yielded similar results. With the exact data set, CNLS DSD fitting of the transformed, subtracted data yielded an S_F value of about 0.044, not a good fit value for exact data. But, even more crucially, it was found that the separate S_F values for the real and imaginary parts obtained with full CNLS fitting were about 0.0144 and 0.0612. Separate fitting of the real-part of the data yielded a value of about 0.0056, and no separate converged fit of the imaginary part was found to be possible. With the data containing 2% random errors, similar results were observed but with a much larger ratio between the CNLS real and imaginary S_F values. The LAS-data DSD KWW fit led to an S_F value of about 0.23, with real and imaginary values of 0.02 and 0.34, and to a separate real-part fit value of 0.01, which dropped to 0.005 when the four lowest frequency points were omitted from the data fitted. These values were very sensitive to the exact value of σ_0 used in the subtraction and led to curves and comparisons much inferior to those plotted in Fig. 14.

The following discrimination procedure now seems reasonable. Suppose one is confronted with a given data set which includes a non-zero σ_0. First, eliminate electrode polarization contributions to the data, if present. If the resulting data set can be adequately fitted using the CSD approach at the ρ-level and at the σ-level, pick the better of the two fits and subtract the effect of the estimated $\sigma_0 = \rho_0^{-1}$ value from the data. These data are then fitted at the dielectric level using the DSD approach with the same or a different dispersion model as that used in the CSD fits. If this fit is poor and of the character of those described above, the original data set most likely arises from CSD. This is very probably the case for the LAS data. Alternatively, one can start with a DSD fit at the σ-level, one including a separate σ_0 parameter, subtract its estimated value and try fitting again without it. The results of these various fitting procedures will often make it obvious whether the data involve CSD, DSD, or perhaps a combination of the two. To test for such combined response, one will need to fit the data with a model including both the DEC and the DED elements shown in Fig. 2.

9. Conclusions

Equations of Moynihan and his associates for the analysis of conductive-system dispersive response are shown to be physically implausible and to arise from incorrect generalization of single-time-constant response to dispersive response. New exact equations are derived to replace the Moynihan ones and their use is demonstrated. In addition, one of them provides a rationale for the approximate Barton, Nakajima, Namikawa (BNN) relation, an empirical equation which has been found to be applicable for much disordered-material frequency-response data.

The use and importance of complex-non-linear-least-squares data fitting is demonstrated for synthetic and experimental frequency- and transient-response data. When fitting is carried out with proportional weighting, exactly the same results are obtained for fitting at the complex resistivity and at the complex modulus levels, settling the argument about which approach is the better. The LEVM fitting program is used both to fit response models to frequency-response data and also to invert such frequency-domain data and time-domain data to obtain estimates of their underlying distribution of relaxation times or activation energies. The role of the high-frequency-limiting dielectric-system dielectric constant, $\epsilon_{D\infty}$, in both inversion and in direct data fitting is clarified. A valuable plotting approach is demonstrated in which each fit point is directly compared to its corresponding datapoint, rather than just comparing a fit line with the data. Thus, the degree of point-to-point fit agreement is much better demonstrated.

The above methods were employed to fit the model-glass LAS frequency-response data of Moynihan and his associates [4,32], and it was shown that a much better fit is possible over the seven-decade span of the data than any previously obtained. Such fitting used the approximate but quite accurate KWW response model incorporated in LEVM, a model which is applicable for a wide range of the fractional exponent, β. To obtain a fit largely limited by the noise in the data, it was necessary to include electrode-polarization circuit elements in the full fitting model. Contrary to conventional wisdom, such polarization effects were found to be important at both the low and the high ends of the measured frequency range. After fitting of the full model, the effects of electrode polarization may be eliminated from the data, and the resulting subtracted-data fitted KWW model response very well over the entire extent of the data. A procedure for helping identify whether frequency-response data involve conductive-system dispersion or dielectric-system dispersion was described and applied to the LAS data. It suggested that these data involved conductive rather than dielectric dispersion.

Appendix A. Comparison of CSD and CTM conductive-system dispersed fitting expressions

I showed in 1985 [6,9], without knowledge of the relevant ground-breaking CTM approach to CSD data analysis [1–5], that if the energy-loss part of a distributed process was distributed but the energy-storage part was not (the usual situation), the same formal DRT or distribution of activation energies expression employed for calculating DSD response, $g_D(\tau)$, could be used for CSD response calculation provided that $g_D(\tau)$ was multiplied by a factor proportional to τ. Some consequences of this unifying approach for the representation and fitting of CSD response are explored here, and a general relation is derived between an arbitrary normalized DSD DRT, $g_D(\tau)$, and the corresponding CSD DRT, $G(\tau) = G_{CD}(\tau)$.

If we replace the Z-level CSD $G(\tau)$ of Eq. (34)

by $\tau g_D(\tau)$ and normalize the new distribution, Eq. (34) becomes

$$I(\omega)=I_{CD}(\omega)\equiv\frac{\int_0^\infty \frac{\tau g_D(\tau)\,d\tau}{[1+i\omega\tau]}}{\int_0^\infty \tau g_D(\tau)\,d\tau}. \quad (A1)$$

However, since the denominator is, by Eq. (4), just $\langle\tau\rangle_D$, we may write [6,9]

$$I_{CD}(\omega)\equiv\int_0^\infty \frac{G_D(\tau)\,d\tau}{[1+i\omega\tau]}, \quad (A2)$$

where

$$G_{CD}\equiv[\tau/\langle\tau\rangle_D]g_D(\tau). \quad (A3)$$

It follows, in terms of $x\equiv\tau/\tau_o$, that

$$\langle x^m\rangle=\langle x^m\rangle_C=\langle x^{m+1}\rangle_D/\langle x\rangle_D. \quad (A4)$$

By contrast, if we instead take $G(\tau)=g_D(\tau)$, then from Eq. (10) $\langle x^m\rangle=\langle x^m\rangle_D$. For the exact KWW $g_D(\tau)$ with fractional $\beta=0.5$, the values of $\langle x^m\rangle_D$ and $\langle x^m\rangle_C$ are [41]: 12, 60; 2, 6; 1, 1; and ∞, 0.5 for $m=2$, 1, 0, and -1, respectively.

For comparison with the original CTM approach, write the M-level response associated with Eq. (A2) in full unnormalized form. The result is

$$M_{CD}(\omega)=\frac{i\omega\epsilon_V\rho_{C\infty}+[\epsilon_V\Delta\rho/\langle\tau\rangle_D]}{\int_0^\infty\left[1-\frac{1}{[1+i\omega\tau]}\right]g_D(\tau)\,d\tau}$$

$$=i\omega\epsilon_V\rho_{C\infty}+[\epsilon_V\Delta\rho/\langle\tau\rangle_D][1-I_D(\omega)], \quad (A5)$$

one which can be directly used for fitting when the form of $I_D(\omega)$ is known. Consider now the less general $\rho_{C\infty}\to 0$ case treated earlier by CTM. It then follows from Eqs. (20) and (A4) that

$$[\epsilon_V\Delta\rho/\langle\tau\rangle_D]\to\epsilon_V\rho_0\langle\tau^{-1}\rangle_C=1/\epsilon_{C\infty}. \quad (A6)$$

Comparison of Eq. (A5) (re-written using Eq. (A6)) with the CTM Eq. (37) expression shows that the $\epsilon_{D\infty}$ appearing in Eq. (37) is incorrect and must be replaced by $\epsilon_{C\infty}$. Such replacement in the CTM Eq. (1) corrects it and makes it consistent with the CSD Eq. (20). Further, because CTM used $\epsilon_{D\infty}$ in their analyses instead of $\epsilon_{C\infty}$, the -1 term in their Eqs. (3) and (6) must be eliminated. Then, for example, one obtains

$$\epsilon_{C0}/\epsilon_{C\infty}=\langle x^2\rangle_D[\langle x\rangle_D]^{-2}=\langle x\rangle_C\langle x^{-1}\rangle_C. \quad (A7)$$

Note that $\epsilon_{D\infty}$ does not appear in any of the above purely CSD relations. It must be treated as a separate fitting parameter (i.e., not a part of $I_{CD}(\omega)$ or $I_D(\omega)$) whether DSD response is present or not. Here, we shall use $\epsilon_{D\infty}$ to mean the ordinary dielectric-system contribution to the total high-frequency-limiting dielectric constant, $\epsilon_\infty\equiv\epsilon_{C\infty}+\epsilon_{D\infty}$, wherever possible (but see the Class-B discussion below). When CNLS fit parameters have been estimated, LEVM extrapolation of the fitting model may be used to obtain the values of ϵ_0, ϵ_∞, and ρ_0 consistent with the model and its parameter estimates. Incidentally, the approximate KWW model does not involve sufficiently accurate behavior of $[1-I_D(\omega)]$ in the $\omega\to 0$ limit to allow adequate ϵ_0 extrapolation for CTM fits.

It is useful to distinguish between two different classes of CSD fitting models, A and B. Class A involves all those models which involve finite and non-zero values of ϵ_{C0} and $\epsilon_{C\infty}$ as intrinsic parts of their response, such as the Gaussian and the cutoff-exponential distributions of activation energies models [6,9], and the exact $\beta=0.5$ KWW model. These models are just those that arise from the integrations of Eqs. (A2) and (A5) or are consistent with them. The analysis shows that, for such models, $\epsilon_{C\infty}$ is properly non-zero. Synthetic data calculated using the corrected CTM approach can be fitted exactly by Class A models. Eqs. (11)–(26) apply to I_{CD} Class-A fit results with all $\langle x^m\rangle$ quantities replaced by the $\langle x^m\rangle_C$. For Class-A LEVM fitting, one will directly obtain a non-zero estimate of the separate $\epsilon_{D\infty}$ parameter if the data allow it to be adequately distinguished. Let $\epsilon_\tau\equiv(\tau_o/\epsilon_V\rho_0)$, a quantity whose value may be calculated from the parameter estimates. Eqs. (16) and (20) apply using the $\langle x^m\rangle_C$ parameters of Eq. (A4), thus allowing $\epsilon_{C0}=\epsilon_0-\epsilon_{D\infty}=\epsilon_\tau\langle x\rangle_C$ and $\epsilon_{C\infty}=\epsilon_\infty-\epsilon_{D\infty}=\epsilon_\tau[\langle x^{-1}\rangle_C]^{-1}$ to be determined from the fit value of $\epsilon_{D\infty}$ and the extrapolated values of ϵ_0 and ϵ_∞, all consistent with Eq. (A7).

These results also allow one to obtain estimates of $\langle x \rangle_C$ and $\langle x^{-1} \rangle_C$.

The situation is somewhat different for Class B models, those for which $\epsilon_{C\infty} = 0$, such as the empirical Cole–Cole, Cole–Davidson, and Havriliak–Negami models. Class B models are generally less complete and less appropriate for CSD data fitting than are Class A ones. The present approximate KWW model without cutoff is also a member of Class B because it involves the Havriliak–Negami function as part of its response [36]. It is helpful to define two different Class-B situations. The first, which will be denoted by CSD, is that where Eq. (34) or (38) is used for fitting, and it either directly involves known $I(\omega) = I_D(\omega)$ models or the direct use of a known $g_d(\omega)$ expression. The second type, which will be identified by CTM, involves the use of $I_D(\omega)$ in Eq. (A5) for fitting.

Since most of the fitting of experimental data presented herein involves Class-B models, it is important to distinguish their similar and dissimilar responses. First, important relations may most simply be expressed in terms of the $\langle x^m \rangle_D$ quantities. For the CSD approach, fitting of CSD data involving $\epsilon_{D\infty} \neq 0$ (the case for all real data), one finds that the free $\epsilon_{D\infty}$ parameter actually estimates ϵ_∞, rather than just $\epsilon_{D\infty}$, so no separate estimate of $\epsilon_{C\infty}$ is available. For the CTM situation, however, an estimate of $\epsilon_{C\infty}$ is directly obtained, as well as a useful estimate of $\epsilon_{D\infty}$ when its estimate is non-zero. Unfortunately, for limited-range experimental data, it is frequently found that the $\epsilon_{C\infty}$ estimate cannot be adequately distinguished from that of ϵ_∞. Because it is often observed for disordered solids that ϵ_∞ fit estimates (usually identified as dielectric-system $\epsilon_{D\infty}$ contributions [1,2]) are larger than those expected from pure dielectric processes, and may be as large as 20 or more [32], it is likely that the $\epsilon_{C\infty}$ part of an unresolved ϵ_∞ sum is dominant in many such cases.

For Class-B CSD fit analysis, a direct estimate of ρ_0 is available but none of $\epsilon_{C\infty}$, while for CTM analysis a direct estimate of $\epsilon_{C\infty}$ is available but none of ρ_0 unless Eq. (A5) is used for fitting. However, the use of the directly estimated parameter values and extrapolation values, along with the equations $\epsilon_{C\infty} = \epsilon_\infty - \epsilon_{D\infty} = \epsilon_\tau \langle x \rangle_D$ and $\epsilon_{C0} = \epsilon_0 - \epsilon_{D\infty} = \{\langle x^2 \rangle_D / [\langle x \rangle_D]^2\} \epsilon_{C\infty}$, allows useful estimates of all relevant quantities to be obtained when a value of $\epsilon_{D\infty}$ is available, and it yields less complete estimates when $\epsilon_{D\infty}$ is unknown. The preceding equations have been employed in the fit calculations in the text, and when a choice was needed to be made between alternate relations, that which seemed most plausible for the particular data being analyzed was used. CNLS fitting of CSD data with Class-B models is illustrated by the results in Tables 2–4. When $\epsilon_{D\infty}$ cannot be separately estimated and is unknown but is expected to be significant, Class-B fitting is likely to be unsatisfactory, and one should use accurate Class-A fit models with appropriate weighting wherever possible.

Appendix B. Principal acronyms and subscripts

BNN	Barton, Nakajima, and Namikawa equation
C	Subscript denoting conductive or continuous
CD	Cole–Davidson response model
CNLS	Complex non-linear least squares
CSD	Conductive-system dispersion; also the CSD fitting approach
CTM	C.T. Moynihan and associates and their corrected fitting approach
CV	Continuous distribution, variable (free)-τ DRT fitting method
D	Subscript denoting dielectric or discrete
DF	Discrete distribution, fixed (constant)-τ DRT fitting method
DRT	Distribution of relaxation times
DSD	Dielectric-system dispersion
DV	Discrete distribution, variable (free)-τ DRT fitting method
IS	Immittance (or impedance) spectroscopy
KWW	Kohlrausch–Williams–Watts fractional-exponential response model
LAS	$Li_2O–Al_2O_3–2SiO_2$ glass
LEVM	The CNLS computer fitting program used herein
PWT	Proportional weighting (in least squares fitting)
SD	Standard deviation. That for a fit is denoted S_F
UWT	Unity weighting (in least squares fitting)
V	Subscript denoting vacuum or variable

Appendix C. The $\beta = 0.5$ KWW cut-off distribution

Physical realizability requires that all valid response functions must lead to complex-plane ρ or ϵ plots that intersect the real axis at a 90° angle at both low and high frequencies [42,72], in agreement with the limiting responses of Eqs. (11)–(14). Many empirical response models, including the KWW one, do not satisfy this requirement. The GBEM effective-medium model [38,65], the jump-relaxation model [73] and the Gaussian model [7,8], however, do so. In addition, in current work I have shown that a recently proposed model involving Coulomb fluctuations [74] also leads to exact Gaussian response [75].

Lack of realizability may be cured by cutting off the model DRT response at the extremes of the relaxation-time range. Usually a sharp cutoff is sufficient. KWW response requires such a cutoff only at low τ, say $\tau_{\min}$ (corresponding to the high frequency, $\omega_{\max}$), and the consequences of such a cutoff will be described here. When normalization is enforced for the $\beta = 0.5$ KWW $G(\tau) = g_D(\tau)$ of Eq. (45) by requiring that it be zero for $\tau < \tau_{\min}$ in Eq. (9), one obtains the following result in terms of the normalized τ variable $x \equiv \tau/\tau_0$,

$$G_x(x) = \begin{cases} \left[\Gamma(\tfrac{1}{2})/\Gamma(\tfrac{1}{2}, x_{\min}/4)\right] \\ \times(4\pi x)^{-1/2}\exp(-x/4) & (x_{\min} \le x \le \infty), \\ 0 & (0 \le x < x_{\min}), \end{cases} \tag{C1}$$

where $\Gamma(\frac{1}{2}, x_{\min}/4)$ is an incomplete gamma function and $\Gamma(\frac{1}{2}, 0) = \Gamma(\frac{1}{2}) = \sqrt{\pi}$ the ordinary gamma function. It follows from Eqs. (C1) and (10) that

$$\langle x^m \rangle_D = 4^m \Gamma(m + \tfrac{1}{2}, x_{\min}/4)/\Gamma(\tfrac{1}{2}, x_{\min}/4), \tag{C2}$$

consistent with the arbitrary-β, $x_{\min} = 0$ result, $\beta^{-1}\Gamma(m/\beta)/\Gamma(m)$ of Ref. [41].

Since $x_{\min}$ will generally be very much smaller than unity, we may use the first terms of a series expansion of the incomplete gamma function to obtain a useful approximation for this function. This is $\Gamma(\nu, z) \simeq \Gamma(\nu)[1 - \exp(-z)z^{\nu}/\Gamma(\nu + 1)]$. For small z, it is only significantly different from $\Gamma(\nu)$ for $\nu < 1$. It follows that the term in square brackets in Eq. (C1) may then be well approximated by $[1 - (x_{\min}/\pi)^{1/2}]^{-1}$. We also obtain the approximation

$$\langle x^m \rangle_D \simeq 4^m \frac{\Gamma(m + \frac{1}{2})\left[1 - (x_{\min}/4)^{m+1/2}/\Gamma(m + \frac{3}{2})\right]}{\sqrt{\pi}\left[1 - (x_{\min}/\pi)^{1/2}\right]}, \tag{C3}$$

which properly leads to $\langle x^0 \rangle_D = 1$. To first order, one also obtains $\langle x \rangle_D \simeq 2[1 + (x_{\min}/\pi)^{1/2}]$, and $\langle x^{-1} \rangle_D \simeq (\pi x_{\min})^{-1/2} + (\pi^{-1} - 0.5)$. Thus, for small $x_{\min}$ the quantity $\langle x^{-1} \rangle_D$ will be very large and $\langle x^{-2} \rangle_D$, proportional to $(x_{\min})^{-3/2}$, will be much larger still.

References

[1] P.B. Macedo, C.T. Moynihan and R. Bose, Phys. Chem. Glasses 13 (1972) 171.

[2] V. Provenzano, L.P. Boesch, V. Voltera, C.T. Moynihan and P.B. Macedo, J. Am. Ceram. Soc. 55 (1972) 492.

[3] J.H. Ambrus, C.T. Moynihan and P.B. Macedo, J. Phys. Chem. 76 (1972) 3287.

[4] C.T. Moynihan, L.P. Boesch and N.L. Laberge, Phys. Chem. Glasses 14 (1973) 122.

[5] F.S. Howell, R.A. Bose, P.B. Macedo and C.T. Moynihan, J. Phys. Chem. 78 (1974) 639.

[6] J.R. Macdonald, J. Appl. Phys. 58 (1985) 1955.

[7] J.R. Macdonald, J. Appl. Phys. 61 (1987) 700.

[8] J.R. Macdonald, J. Appl. Phys. 62 (1987) R51. [1]

[9] J.R. Macdonald and J.C. Wang, Solid State Ionics 60 (1993) 319.

[10] J.R. Macdonald, J. Appl. Phys. 75 (1994) 1059.

[11] J.R. Macdonald, ed., Impedance Spectroscopy – Emphasizing Solid Materials and Systems (Wiley–Interscience, New York, 1987).

[12] M. Pollak and T.H. Geballe, Phys. Rev. 122 (1961) 1742.

[13] S.R. Elliott, Philos. Mag. 36 (1977) 1291.

[14] S.R. Elliott, Adv. Phys. 36 (1987) 135.

[15] F. Henn, S.R. Elliott and J.C. Giuntini, J. Non-Cryst. Solids 136 (1991) 60.

[16] A. Hunt, J. Non-Cryst. Solids 160 (1993) 183.

[1] The KWW distribution is misidentified here as a stable Lévy distribution; instead it is the characteristic function of such a distribution.

[17] J.R. Macdonald and M.K. Brachman, Rev. Mod. Phys. 28 (1956) 393.
[18] S.R. Elliott, Solid State Ionics 27 (1988).
[19] J. Schrama, PhD thesis, University of Leiden (1957).
[20] D.P. Almond and A.R. West, Solid State Ionics 11 (1983) 57.
[21] J.C. Dyre, J. Appl. Phys. 64 (1988) 2456.
[22] Discussion session: Glassy Ionics, J. Non-Cryst. Solids 131–133 (1991) 1118.
[23] S.R. Elliott, J. Non-Cryst. Solids 170 (1994) 97.
[24] J.R. Macdonald and L.D. Potter Jr., Solid State Ionics 23 (1987) 61. [2]
[25] J.R. Macdonald, Electrochim. Acta 35 (1990) 1483
[26] B.A. Boukamp and J.R. Macdonald, Solid State Ionics 74 (1994) 85.
[27] J.R. Macdonald, J. Chem. Phys. 102 (1995) 6241.
[28] R.H. Cole and E. Tombari, J. Non-Cryst. Solids 131–133 (1991) 969.
[29] H.K. Patel and S.W. Martin, Phys. Rev. B45 (1992) 10292.
[30] B.S. Lim, A.V. Vaysleyb and A.S. Nowick, Appl. Phys. A56 (1993) 8.
[31] R. Diaz Calleja, J. Non-Cryst. Solids 172–174 (1994) 1413.
[32] C.T. Moynihan, J. Non-Cryst. Solids 172–174 (1994) 1395.
[33] J.R. Macdonald, J. Electrochem. Soc. 124 (1977) 1022.
[34] J.R. Macdonald, A. Hooper and A.P. Lehnen, Solid State Ionics 6 (1982) 65.
[35] J.R. Macdonald and G.B. Cook, J. Electroanal. Chem. 168 (1984) 335; 193 (1985) 57.
[36] J.R. Macdonald and R.L. Hurt, J. Chem. Phys. 84 (1986) 496.
[37] J.R. Macdonald, Solid State Ionics 58 (1992) 97.
[38] J.R. Macdonald, Appl. Phys. A59 (1994) 181.
[39] J.R. Macdonald, J. Electroanal. Chem. 378 (1994) 17. [3]
[40] C.J.F. Bottcher and P. Bordewijk, Theory of Electric Polarization, Vol. II (Elsevier, Amsterdam, 1978). [4]
[41] C.P. Lindsey and G.D. Patterson, J. Chem. Phys. 73 (1980) 3348. [5]
[42] J.R. Macdonald, Solid State Ionics 25 (1987) 271.
[43] R. Kohlrausch, Pogg. Ann. Phys. Chem. 91 (2) (1854) 179.
[44] G. Williams amd D.C. Watts, Trans. Faraday Soc. 66 (1970) 80.

[2] Version 6.1 of the LEVM fitting program may be obtained from Solartron Instruments, UK, +44-1252 376 666, e-mail: briansayers100444.3217@compuserve.com.

[3] The word 'relation' in the title of this paper should be 'relaxation'.

[4] The lower limits of the integrals in Eqs. (9.1)–(9.4) should be $-\infty$, not 0.

[5] The $G(\tau)$ and $\rho(\tau)$ functions introduced in this excellent DSD work are equivalent to the present $F(y)$ and $G(\tau)$ functions, respectively.

[45] G. Williams, D.C. Watts, S.B. Dev and A.M. North, Trans. Faraday Soc. 67 (1971) 1323.
[46] J.L. Barton, Verres Refract. 20 (1966) 328.
[47] T. Nakajima, in: 1971 Annual Report, Conference on Electric Insulation and Dielectric Phenomena (National Academy of Sciences, Washington, DC, 1972) p. 168.
[48] H. Namikawa, J. Non-Cryst. Solids 18 (1975) 173.
[49] R.A. Huggins, in: Diffusion in Solids, Recent Developments, ed. A.S. Nowick and J.J. Burton (Academic Press, New York, 1975) p. 445.
[50] S.W. Martin and C.A. Angel, J. Non-Cryst. Solids 83 (1986) 185.
[51] F. Stickel, E.W. Fischer and R. Richert, J. Chem. Phys. 102 (1995) 6251.
[52] K.W. Wagner, Ann. Phys. 4-40 (1913) 817.
[53] J.R. Macdonald and C.A. Barlow Jr., Rev. Mod. Phys. 35 (1963) 940.
[54] I.M. Hodge and C.A. Angell, J. Chem. Phys. 67 (1977) 1647.
[55] K.L. Ngai and U. Strom, Phys. Rev. B27 (1983) 6031.
[56] K.L. Ngai and H. Jain, Solid State Ionics 18–19 (1986) 362.
[57] K.L. Ngai, J.N. Mundy, H. Jain, O. Kanert and G. Balzer-Jollenbeck, Phys. Rev. B39 (1989) 6169.
[58] P. Sarkar and P.T. Nicholson, J. Phys. Chem. Solids 50 (1989) 197.
[59] H.K. Patel and S.W. Martin, Phys. Rev. B45 (1992-II) 10292.
[60] W.C. Hasz, C.T. Moynihan and P.A. Tick, J. Non-Cryst. Solids 172–174 (1994) 1363.
[61] H. Jain and C.H. Hsieh, J. Non-Cryst. Solids 172–174 (1994) 1408.
[62] C.K. Majumdar, Solid State Commun. 9 (1971) 1087.
[63] J.-S. Lee and H.-I Yoo, J. Electrochem. Soc. 142 (1995) 1169.
[64] W.J. Thompson and J.R. Macdonald, Proc. Nat. Acad. Sci. USA 90 (1993) 6904.
[65] J.R. Macdonald, Phys. Rev. B49 (1994-II) 9428.
[66] D.W. Davidson and R.H. Cole, J. Chem. Phys. 19 (1951) 1484.
[67] G.P. Johari and K. Pathmanathan, Phys. Chem. Glasses 27 (1988) 219.
[68] C.T. Moynihan, private communication.
[69] S. Havriliak Jr. and S. Negami, J. Polym. Sci. C14 (1966) 99; J. Non-Cryst. Solids 172–174 (1994) 297.
[70] H.P. Schwan, in: Advances in Biological and Medical Physics, ed. J.H. Lawrence and C.A. Tobias (Academic Press, New York, 1957) pp. 147–209.
[71] J.C. Wang, Electrochim. Acta 33 (1988) 707.
[72] R. Syed, D.L. Gavin, C.T. Moynihan and A.V. Lesikar, J. Am. Ceram. Soc. 64 (1981) C118.
[73] K. Funke, Prog. Solid State Chem. 22 (1993) 111.
[74] V.N. Bondarev and P.V. Pikhitsa, Phys. Lett. A196 (1994) 247.
[75] J.R. Macdonald, submitted to Phys. Lett. A.